Physics – Uspekhi **67** (7) 639 – 667 (2024)

REVIEWS OF TOPICAL PROBLEMS PACS number: 96.50.S –

Direct observations of cosmic rays: state of the art

A D Panov, D M Podorozhnyi, A N Turundaevskii

DOI: https://doi.org/10.3367/UFNe.2023.11.039589

Contents

Abstract. The state of the art in exploring galactic cosmic rays using spacecraft and high-altitude balloons is reviewed in detail. The most urgent basic problems of high- and ultrahigh-energy astrophysics, solved by direct observations of cosmic rays, are discussed. Prospects for the advancement of research in this field of science in the next decade are outlined.

Keywords: cosmic rays, direct observations

1. Introduction

Galactic cosmic rays (GCRs) are fluxes of relativistic and ultra-relativistic charged particles that fill interstellar space. The cosmic rays consist of hadronic and leptonic components. The hadronic (otherwise referred to as nuclear) component of GCRs consists of nuclei of chemical elements ranging from protons (hydrogen nuclei) to nuclei much heavier than iron. The lepton component consists of electrons and positrons. Although the hadron component is strongly dominant, the presence of the lepton component is also very important for understanding the nature of cosmic rays, since it can contain important information about nearby cosmic ray sources and exotic objects such as dark matter or primordial black holes. Cosmic rays also contain antimatter in the form of antiprotons and possibly heavier antinuclei. Relativistic cosmic particles may also contain some hypothetical exotic objects, such as strangelets [1, 2].

The nuclear constituents of galactic cosmic rays is one of the most important constituents of the interstellar medium, since the corresponding spatial energy density (about 1.5 eV cm^{-3} [3]) is comparable to that of the interstellar electromagnetic radiation field (from the microwave background to the ultraviolet radiation of stars: in total, about 1 eV cm^{-3} [4]), with a magnetic field energy density (a field of 6 μG in the solar region [5] corresponds to an energy density of about 1 eV cm^{-3}) and with an average kinetic energy density of interstellar gas ($\sim$ 1 eV cm^{-3} [6, p. 185; 7, p. 208]). In this sense, cosmic rays are one of the main components of outer space, and the physics of cosmic rays requires in-depth study to understand the world around us, i.e., our Galaxy. This explains the natural general scientific interest in cosmic rays.

The most likely source of most cosmic rays is considered to be supernova explosions in our Galaxy [6]. The astrophysics of supernovae is of great interest for many reasons. Supernovae are the source of heavy chemical elements of which terrestrial planets and ourselves consist. Supernova explosions represent one of the most significant phases in the evolution of large stars, as a result of which relativistic astrophysical objects such as neutron stars and black holes can be formed. These objects and the ways they form are of great interest per se, since they are associated with problems that lead to the boundaries of current concepts of space, time, and matter. Explosions of nearby supernovae could have had

A D Panov [a], **D M Podorozhnyi** [b], **A N Turundaevskii** [c]
Skobeltsyn Institute of Nuclear Physics, Lomonosov Moscow State University, Leninskie gory 1, str. 2, 119991 Moscow, Russian Federation
E-mail: [a] panovenator@gmail.com, [b] dmpo@bk.ru, [c] ant@eas.sinp.msu.ru

Received 24 July 2023, revised 29 October 2023
Uspekhi Fizicheskikh Nauk **194** (7) 681 – 710 (2024)
Translated by M Zh Shmatikov

a significant impact on the course of biological evolution on Earth in the past and may have such an impact in the future, which is of importance. In this sense, from a purely practical point of view, we need to have a good understanding of what types of supernovae exist, what impacts can be associated with their explosions, and what can be expected from our immediate stellar environment. From this perspective, nearby sources of cosmic rays are of particular interest. Since supernova explosions appear to be the main source of galactic cosmic rays, cosmic rays can and do provide a large amount of information about the physics of supernovae. Recently, interest has shifted to studying the fine structure of the kinetic energy spectra of cosmic ray nuclei and the subtle features of the chemical composition of cosmic rays. The features of the spectra encode subtle details of the physics of supernova explosions and the process of cosmic ray acceleration, for example, the presence of various types of supernovae with different maximum acceleration energies and different source compositions. It should be noted that alternative sources and mechanisms of cosmic ray acceleration have also been proposed and discussed [8–11]. A comprehensive up-to-date review on the sources and mechanisms of acceleration of CRs is presented in [11].

The propagation of cosmic rays in the Galaxy is significantly determined by the properties of the interstellar medium and the structure of the Galaxy; therefore, some features of the spectra of cosmic rays make it possible to obtain data on the magnitude and structure of interstellar magnetic fields, the density of interstellar matter, the presence and extent of the magnetic halo of the Galaxy, matter flows, etc.

Although leptons (electrons and positrons) represent only a small fraction of the cosmic ray flux (on the level of a percent or less, depending on energy), the study of the leptonic component is of particular interest, which is explained by two main circumstances. First, electrons and positrons from cosmic rays may be products of the annihilation or decay of dark matter particles, which should exhibit a corresponding signature in the spectra of positrons and electrons and may shed light on the nature of dark matter. Second, leptons, due to their low mass and large energy losses due to synchrotron radiation and inverse Compton scattering, cannot, unlike cosmic ray nuclei, propagate over galactic distances. Therefore, cosmic ray leptons carry important information about nearby sources of electrons and positrons, such as supernova remnants or pulsars, which can also produce a certain signature in the energy spectra of cosmic ray leptons in the form of their specific fine structure [12, 13]. It is significant that the signatures of dark matter can, in principle, be distinguished from the structures associated with nearby sources. At present, some anomalies in the behavior of the spectra of electrons and positrons of cosmic rays are already known, but data are not sufficient to unambiguously determine their nature.

V L Ginzburg and S I Syrovatskii hypothesized in their fundamental monograph [6] that the energy spectrum of particles accelerated in supernova shells may feature a universal power-law character with an exponent close to -2.5 [6, p. 323–326], and this is "a fundamental property of the dynamics of turbulent magnetized plasma in space conditions" [6, p. 321]. This conclusion was made on the basis of simple qualitative considerations, assuming an equal distribution of energy among cosmic rays, the magnetic field, and the turbulent movement of gas in the supernova envelope. Later, G F Krymskii [14] and A R Bell [15, 16] directly showed that the acceleration of particles according to the Fermi mechanism of the first kind at the front of the shock wave of the supernova shell actually leads to a power-law energy spectrum with an exponent close to the universal value $-(2 + 4/\mathrm{M}^2)$, where $\mathrm{M} \gg 1$ is the Mach number of the shock wave (see also [17–19]). The exponent of the spectrum of accelerated particles turns out to be slightly larger than two (on a scale value of 0.1–0.2), and observed spectra with an exponent close to -2.7 are easily obtained under the assumption that the length of the diffusion escape of particles from the Galaxy is a power-law function of the magnetic rigidity of the particle with an index of about -0.5. Since virtually all experimental data obtained before 2000 fit very well into such a model, it de facto acquired the status of a 'standard model' of cosmic ray physics. The main feature of this model is that the power-law magnetic rigidity spectra are the same for all nuclei in the source. This paradigm does not have a generally accepted name; for example, in [20] it is referred to as a 'reference scenario,' but it is used very often, and it is always clear what is meant. Later, the shock wave acceleration model was further developed, in particular, by introducing the mechanism of nonlinear magnetic field amplification [21], which made it possible to explain the acceleration of cosmic rays in supernova shells at least up to the cosmic ray knee region [22, 23]. This, however, did not alter the essence of the standard model.

Since as early as the 1950s, it has been known that one of the main features of the energy spectrum of cosmic rays (more precisely, the spectrum of all particles in terms of energy per particle) is a kink (knee) at energies between 10^{15} and 10^{16} eV [24] on a background of, as a whole, approximately power-law behavior of the spectrum. This spectral feature is known as the Kulikov–Christiansen knee. However, in the 2000s, it became clear that even at lower energies the spectra of cosmic rays have many features that violate the simple universal power-law behavior of the 'standard model.' The first such feature was the difference in the slopes of the spectra of protons and helium at energies from approximately 100 GeV to 10 TeV, which was first confirmed with high statistical significance (about 10σ) in the ATIC experiment [25]. Later, the effect was confirmed in the experiments CREAM [26–28], PAMELA [29], AMS-02 [30, 31], etc. The ATIC collaboration [32], by solving the inverse particle propagation problem, found with a statistical confidence of 3.2 standard deviations a systematic growth in the spectral slope from helium to iron in the source with increasing nuclear charge for the magnetic rigidity range from 50 to 1350 GV, which also violates the simple universal power-law behavior of spectra. ATIC experiment [33] was the first to note that the shape of the spectra of protons and helium at energies from 50 GeV to about 10 TeV significantly differs from the power-law form by a pronounced decrease in slope at energies between 100 GeV and 1 TeV. The ATIC experiment also discovered a similar inflection in the spectra of heavier abundant nuclei [33, 34]. These inflections were later confirmed by the results of CREAM [35], PAMELA [29], and AMS-02 [30, 31]. Thus, at energies below the Kulikov–Christiansen knee, the spectra of CRs exhibit a number of features that violate the 'standard model' of CR physics, which should be carefully studied, since they encode the physics of CR sources and propagation in the Galaxy.

Experiments in cosmic ray physics are divided into direct experiments (stratospheric or cosmic), in which information

is obtained as a result of direct contact of measuring equipment with a cosmic particle, and ground-based experiments, in which high-energy cosmic rays are observed indirectly through cascades of secondary particles in the atmosphere, which are called extensive atmospheric showers (EASs). The advantage of EAS methods over direct methods is that the former make it possible to measure the spectra of cosmic rays up to extremely high energies (scale of 10^{21} eV), when particle fluxes are very small; therefore, for direct measurements, with their significantly smaller geometric factors of instruments, the statistics are insufficient. In the region of the Kulikov–Christiansen knee (~ 3 PeV per particle), data have so far been obtained exclusively from EAS experiments (for a review of recent results, see [36]). These data currently provide high statistical significance and reliability in measuring the energy spectrum of all particles, but contain only very poor averaged information on the chemical composition of nuclei, without providing element-by-element resolution of charge spectra. Although very good matching of direct and EAS measurement data for the all-particle spectrum has recently been achieved [37], the element-wise structure of the 3-PeV knee remains unknown, which greatly complicates the interpretation of this most important feature of the cosmic ray spectrum. Unlike EAS techniques, direct measurements usually provide element-wise resolution of charge spectra (and sometimes even the isotopic composition of CRs (see Section 7)). Therefore, information about numerous features of CR spectra at lower energies (currently, below or on the order of 100 TeV per particle) turns out to be much more detailed than EAS experiments can obtain in their energy region.

In this review, we present the current state of cosmic ray research that uses direct methods. We focus less on the compilation of the results of modern direct experiments in cosmic ray physics but rather on an analysis of the main unsolved problems and hot spots of this field of science. The selection of basic facts for such a review is inevitably affected by the preferences of the authors, so the review does not claim to be complete. We also emphasize that the review was written by experimenters working in this field and is dedicated specifically to the experimental side of the matter. A vast literature is available, which is devoted to the theoretical analysis of the phenomena under discussion, especially in relation to the spectra of electrons, positrons, and antiprotons. All this work is barely touched upon by this review, except in cases when they are an absolute must. Nor does the review consider the problems of high-energy gamma-ray astronomy using space-based instruments, although very often the same space observatories are used concurrently in both cosmic ray physics and gamma-ray astronomy (Fermi, CALET, DAMPE; see Section 2). It is not possible to include all this information in a single review.

Section 2 provides an overview of the main state-of-the-art instruments for direct observations of cosmic rays, which are mentioned in subsequent sections of the review. Section 3 examines the experimental status of the recently discovered 'universal small knee' of cosmic rays near a magnetic rigidity of 10 TV. Section 4 considers the different behaviors of the spectra of cosmic ray nuclei with different charges in various aspects of this problem. Section 5 discusses the still unsolved enigma in the behavior of light secondary nuclei Li, Be, B. Section 6 is also devoted to the behavior of the spectra of nuclei in which the proportion of the secondary component is large, but here it refers primarily to heavier nuclei from the 'sub-iron' group with charges of approximately 18 to 24. Section 7 discusses problems in observing superheavy nuclei (heavier than nickel) and the isotopic composition of cosmic ray nuclei, which is closely related to superheavy nuclei according to the instruments used. Section 8 is devoted to the problems of the spectra of the lepton component of cosmic rays (electrons and positrons) and the closely related topic of hadronic antimatter in cosmic rays (antiprotons, antihelium).

The main part of the review lists a large number of unsolved problems in cosmic ray physics and outlines the requirements for hardware necessary to advance in solving them. Therefore, the sections of the review from 3 to 8 can be considered an extended formulation of the issue presented in Section 9, the last section of the review, which displays some promising projects aimed at solving the formulated problems.

2. State-of-the-art instruments for direct measurements of cosmic rays

By state-of-the-art instruments for direct observations of cosmic rays we primarily mean those that are currently operational, that are continuing to collect data, or for which data processing and publication of new results are ongoing. To some extent, the ATIC and CREAM experiments of the early 2000s should also be considered modern instruments, since they were the first to convincingly demonstrate the presence of a complex structure of cosmic ray spectra at energies below the Kulikov–Christiansen knee (see Section 1), which laid the foundation for the modern stage in direct measurements of CRs. For some areas of direct CR measurements, new instruments have not appeared for a long time, and, in this case, by modern instruments we mean those that have given the most recent results in their field. This is the situation in measurements of the charge and isotopic composition of superheavy nuclei (heavier than a nickel nucleus).

There are many similarities in the design of different instruments (spectrometers) intended for observing high-energy cosmic rays. Such instruments, at least, should include a system for measuring the charge of the particles and a system for measuring their energy or magnetic rigidity. In addition, the instrument designs provide a number of auxiliary systems, such as anti-coincidence systems for background protection and various track detectors, and, in some cases, provide redundancy of the information for cross-checking data and controlling systematic errors.

A typical representative of the family of instruments designed for direct observations of high-energy cosmic rays is the NUKLON space observatory [38]. A simplified setup of the instrument and a typical 'portrait' of the event are shown in Fig. 1. The particle enters the instrument through the top of the device, where it interacts with a charge detector consisting of four planes, each measuring 50×50 cm^2. Each plane is a matrix of 32×32 silicon detectors, each measuring 1.5×1.5 cm^2. The high degree of segmentation of the detector makes it possible to distinguish the energy deposit of the primary particle from the signals of particles scattered from the instrument in the opposite direction (so-called reverse currents). The trigger for recording an event is generated by three double planes of strip scintillation detectors. The NUKLON Observatory supports two independent methods for determining particle energy. First, there is a conventional and long-known method based on the use of

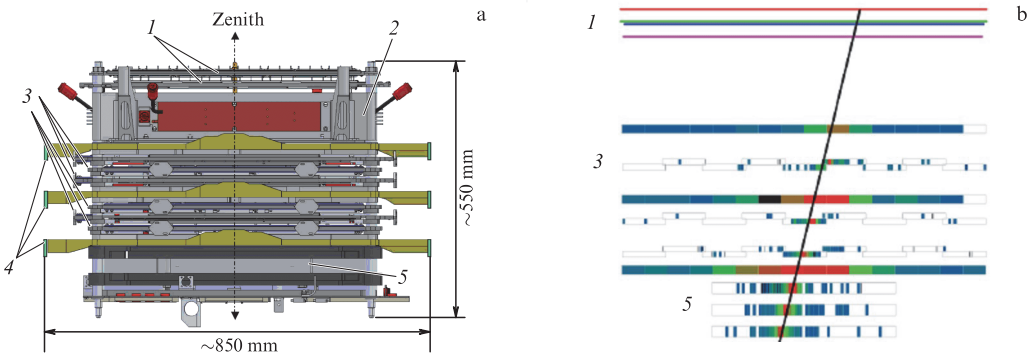

Figure 1. (a) Simplified schematic of NUKLON space spectrometer. *1* — two pairs of planes of charge measurement system; *2* — carbon target; *3* — six planes of energy measurement system using the KLEM method (KLEM tracker); *4* — three double planes of trigger generation system; *5* — calorimeter; (b) 'Portrait' of an event of the NUKLON spectrometer (more precisely, one projection of the portrait). Incident nucleus triggers a nuclear-electromagnetic cascade. Energy deposits in various detectors of spectrometer are presented in conventional colors. Sloped line is a reconstruction of trajectory of a falling nucleus. Numbers *1*, *3*, *5* correspond to designations in panel (a).

an ionization calorimeter [39, 40]. The calorimeter of the NUKLON spectrometer is thin in the sense that deposited in it is only part of the primary particle energy, so reconstructing the particle energy requires a dedicated conversion of the energy deposit into the primary energy, which is a nontrivial task. Second, there is a new kinematic method, KLEM (Kinematic Lightweight Energy Meter), based on measuring the angles of scattering of secondary particles after the first nuclear interaction [41–45]. Thus, the NUKLON spectrometer provides redundant information for determining the energy of particles, while the new KLEM technique corresponds to a geometric factor several times larger than the calorimetric technique, while the conventional calorimetric technique makes it possible to control the operation of the new KLEM. In fact, the main results of the NUKLON spectrometer are obtained using the KLEM method, and the calorimeter provides cross-checking of the correct operation of the equipment. The KLEM technique is associated with six planes of microstrip silicon detectors, which simultaneously operate as a tracker and, together with the energy deposit in the calorimeter, make it possible to reconstruct the initial trajectory of the primary particle. The geometric factor of the NUKLON spectrometer, corresponding to the KLEM technique, is approximately 0.25 m^2 sr (the exact value depends on the particle type); the geometric factor for the calorimeter technique is 3–5 times less (also depends on the type of particles).

The designs of the stratospheric spectrometers ATIC [46, 47] and CREAM [48, 49] and the space observatories Fermi [50], CALET [51–53], and DAMPE [54–57] resemble in their main features the NUKLON observatory described above. All of these instruments include an ionization calorimeter for measuring the primary-particle energy. The calorimeters used are thin for the hadronic component of cosmic rays, while for the lepton component only the Fermi calorimeter is thin, the calorimeters of all other instruments absorbing most of the energy of the primary electron or positron.

In the ATIC and CREAM spectrometers, the charge detectors, similar to the NUKLON spectrometer, are silicon matrices. Furthermore, these spectrometers have additional systems for trigger generation, systems that provide redundancy in charge or energy measurements, etc.

The Fermi observatory is designed primarily for high-energy gamma-ray astronomy, but has shown that it can also measure the spectrum of the lepton component of cosmic rays. The charge detector, which also operates as a tracker, consists of planes of silicon microstrips. Unlike other instruments, the Fermi observatory contains 16 identical units (towers), each of which has its own tracker and calorimeter and is actually an independent instrument. However, data processing algorithms also make it possible to process events when the particle trajectory passes through more than one tower.

In the CALET spectrometer, the charge detector operates based on the use of plastic strip scintillators. In addition to the calorimeter and charge detector, the spectrometer also includes a scintillation-tungsten tracker, based on scintillation fibers (optical fibers), which facilitates reconstructing the particle trajectory and operates as a converter for the production of an electromagnetic and hadron shower in the device. The spectrometer was initially designed to measure the spectrum of electrons and positrons from cosmic rays, but it also demonstrated the capacity to measure the spectrum of nuclei from protons up to nickel, providing important information in the process (see below). It also turned out to be operational as a gamma observatory. The geometric factor of the device for recording high energy electrons is 0.12 m^2 sr.

The DAMPE observatory is a general-purpose system. This instrument was developed both for the study of hadron and electron-positron components of cosmic rays and for high-energy gamma-ray astronomy. Its design is basically the same as that of CALET with some differences, but provides a geometric factor of about 0.3 m^2 sr, which is due to the large size of the instrument. Used as a charge detector, as in the CALET spectrometer, is a plastic strip scintillation detector. Located below is a silicon-tungsten converter-tracker based on the use of silicon microstrips. The DAMPE BGO calorimeter is fully active, since BGO crystals combine the functions of an absorber and a scintillator (the ATIC spectrometer calorimeter was designed in the same way). As an additional system, unlike CALET, the DAMPE spectrometer has a neutron detector located under the calorimeter, which facilitates the separation of cascades from primary leptons and protons (in the latter case, the number of neutrons should be significantly larger).

Unlike the instruments mentioned above (from ATIC to DAMPE), the main element in the PAMELA [58–61] and AMS-02 [62, 63] space observatories is a magnetic spectro-

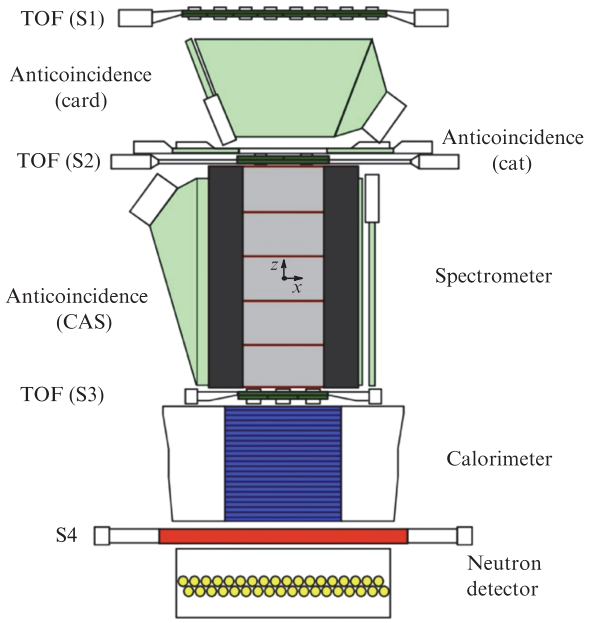

Figure 2. Diagram of PAMELA space spectrometer. Designations in the figure: TOF(S1, S2, S3) — three planes of time-of-flight detector; anti-coincidence — anti-coincidence systems based on scintillators for protection against particles that have not passed through the aperture; spectrometer — magnet containing a system of silicon trackers inside; S4 scintillation 'cascade tail detector' (tail catcher). (Reproduced from [59] with permission of the authors.)

meter for direct measurement of the magnetic rigidity of particles. The block diagrams of PAMELA and AMS-02 are very similar; the devices differ primarily in dimensions and, therefore, in the geometric factor. The block diagram of the PAMELA spectrometer is displayed in Fig. 2. In both cases, the magnetic spectrometer is built on the basis of permanent magnets creating an approximately uniform horizontal magnetic field. Trackers made in both cases on the basis of silicon microstrip planes are placed in a magnetic field. The tracker measures the particle trajectory in a magnet, while the magnetic rigidity of the particle is calculated from the curvature of the path. In addition to the magnetic spectrometer, both space observatories include a thin calorimeter, which is used for auxiliary purposes, notably, to distinguish between ultrarelativistic electrons and antiprotons, and positrons and protons, based on the shape of the calorimeter shower. The tracker in both spectrometers is also the main system for determining the particle charge.

A special class of instruments is represented by stratospheric and space experiments designed to study heavy and superheavy cosmic-ray nuclei. Mentioned among the heavy-nuclei experiments that continue to significantly affect the understanding of cosmic ray physics should be the HEAO-3-C3 experiments (HNE) [64, 65] and TRACER [66–68]. These experiments are focused on measuring the energy spectra of heavy nuclei to the highest possible energies, up to 10 TeV/nucleon. The design of such spectrometers differs significantly from the universal magnetic and calorimetric spectrometers discussed above. Unlike the latter, the equipment of heavy-nuclei experiments should ensure that the nucleus passes through the entire installation without nuclear interaction, i.e., such spectrometers are designed to be very thin for nuclear interactions.

The main goal of the TRACER experiment was to directly measure the energy spectra of nuclei heavier than helium to the highest possible energies, on the order of 10 TeV per nucleon. Since TRACER is a stratospheric balloon spectrometer, and to solve the problem, an exposure of at least ten m^2 sr days is needed, the device efficiency should be very high. The problem was solved by using a technique for particle energy measurement based on a combination of Cherenkov and ionization detectors together with a transition radiation detector. With a device weight of 2.7 tons, its geometric factor was approximately 5 m^2 sr.

To measure nuclear charges, two pairs of detectors (Cherenkov counter + scintillation detector) are used in the upper and lower parts of the device. For each pair of counters, each nucleus is associated with a trajectory on the plane (scintillator signal and Cherenkov counter signal), based on which the charge is determined. The charge is determined separately by the upper pair of detectors and the lower pair of detectors. If the signals match within the limits of statistical fluctuations, the charge determined is calculated as the average. The charge resolution achieved ranges from $0.25e$ for boron to $0.5e$ for iron nuclei.

Energy measurements are performed over an energy region spanning more than four orders of magnitude and are implemented by combining the energy responses of several detectors: a Cherenkov detector, gas proportional tubes dE/dx, and a transition radiation detector (TRD). Proportional counters placed inside the TRD array provide a pure dE/dx signal for particles with a Lorentz factor $\gamma < 400$ and the sum of the dE/dx signal and TRD for faster particles. The proportional counters located on the top of the instrument always provide a clean dE/dx signal. In detecting low-energy particles, an ambiguity arises in the dE/dx readings of detectors (very low-energy particles and high-energy particles yield the same value dE/dx), which is resolved using the signal from the Cherenkov detector. The ambiguity of the dE/dx criterion for determining the energy remained a problem not resolved in the HEAO-3-C3 experiment, which greatly influenced the interpretation of the results of this experiment (see Section 6). The energy resolution of the Cherenkov detector (used for $\gamma < 10$) and the TRD detector in the TRACER experiment (for $\gamma > 400$) is fairly high: 6% and 15%, respectively. In the speed range $10 < \gamma < 400$, the relativistic increase in energy loss of a charged particle in a gas is used to measure energy. Although this growth is quite slow and statistical fluctuations of ionization greatly deteriorate the resolution, especially for light elements, in the TRACER-LDB2 experiment (the second flight of TRACER), optimizing the composition of the gas mixture of proportional counters enabled attaining a resolution from approximately 65% for $Z = 5$ to 40% for $Z = 26$, which made it possible to cover all nuclei from boron to iron by the measurements. In the TRACER-LDB1 experiment (first flight), measurements only started with the oxygen nucleus due to insufficient energy resolution for lighter nuclei.

The HEAO-3-C3 space spectrometer is based on the use of a combination of Cherenkov counters, gas proportional detectors, and hodoscopes composed of multi-wire ionization chambers. The Cherenkov counters were used to determine charge; energy was determined from the relativistic growth of ionization in proportional chambers, and wire hodoscopes were used to determine the trajectory of particles. The spectrometer featured a very large geometric factor. Its exact value, which depended on the problem being solved

and the trigger used, was about 5 m^2 sr. The experiment identified 7.7×10^6 iron nuclei with energies above the Cherenkov counter threshold, which was 1.5 GeV/nucleon. The HEAO-3-C3 device was used to solve primarily two different problems. The first was a detailed measurement of the ratios of the spectra of $Z = 18-28$ nuclei to the spectrum of the iron nucleus up to energies of several hundred GeV/nucleon. In the HEAO-3-C3 spectrometer, Cherenkov counters that operate almost in energy saturation mode are used to determine the particle charge, and its energy is determined using proportional counters based on the relativistic logarithmic growth of ionization losses with increasing particle energy. This technique for determining energy, although enabling energy measurements in a wide range (from several GeV/nucleon to several hundred GeV/nucleon), does not involve an independent calibration. The method is calibrated against flight data by comparing the resulting spectrum of energy deposits in proportional counters for iron nuclei with iron spectra obtained in earlier independent experiments. Therefore, the measured spectrum of iron is not independent, but, as reported by HEAO-3-C3, the measured ratios of the spectra of various nuclei to the spectrum of iron turn out to be virtually independent.

The second task of HEAO-3-C3 was to determine the abundance (charge composition) of superheavy elements $Z \geqslant 30$ in cosmic rays with energies above the setup threshold (0.45 GeV/nucleon for proportional counters or 1.5 GeV/nucleon for Cherenkov detectors) or higher than the geomagnetic threshold (8 GV). Determining the energy spectra of nuclei was not a priority of this experiment. The statistics for superheavy nuclei obtained in the HEAO-3-C3 experiment still remain a record, although the experiment was carried out from 1979 to 1981.

Of the relatively recent specifically superheavy nuclear experiments, we mention the SuperTIGER [69–71], LDEF [72], and ACE-CRIS [73, 74] experiments.

The SuperTIGER stratospheric balloon experiment is aimed primarily at measuring the charge composition of CR nuclei heavier than the iron group up to $Z \approx 60$. Nuclear energy spectra are not measured; the results refer to the entire energy region above the instrument threshold, which is on the order of 1 GeV/nucleon. The spectrometer uses plastic scintillators to measure charge and Cherenkov counters to measure the charge and velocity of nuclei, while scintillation hodoscopes based on optical fibers are employed to reconstruct the trajectory of the primary nucleus. The effective geometric factor of the instrument is ~ 4 m^2 sr (depending on the nucleus), i.e., slightly less than that in the HEAO-3-C3 experiment.

The LDEF experiment is based on the use of solid-state track detectors made of Lexan (plexiglass) polycarbonate plates with a total area of 10.2 m^2 as the main measuring element. The detector was delivered into space on the space shuttle on April 7, 1984 and spent about 6 years in orbit, gaining a total exposure of about 170 m^2 sr years. The results of measurements of the solid-state track detectors were processed after the instrument returned to Earth. Currently, the LDEF experiment provides the highest exposure in the $Z \geqslant 70$ nuclear-charge region.

In 1997, the ACE space station, designed to study the elemental, isotopic, and ionic (charge state) compositions of nuclei in interplanetary space, started operations. One of the six instruments of the ACE mission was the CRIS spectrometric instrument designed to measure the charge composition of nuclei in the range of charges from $Z = 2$ to approximately $Z = 40$ with isotopic resolution of nuclei up to charges of about $Z = 30$ (actually, isotopic resolution for $Z = 32$ [75] was achieved). The CRIS experiment uses a technique based on recording the Bragg peak of the complete stop of nuclei in a stack of thin silicon detectors, together with scintillation trackers used to generate the spectrometer trigger and to reconstruct the particle trajectory. The employed technique limits the nuclear energy range from approximately 50 MeV/nucleon to 500 MeV/nucleon (ranges vary for different nuclei). The exposure time of the spectrometer, which is still in operation, is about 25 years. The small geometric factor of the device (0.025 m^2 sr) is partly compensated by the long exposure time, which made it possible to obtain charge distributions of nuclei up to $Z = 40$ using the CRIS spectrometer. The number of statistics of CRIS charge spectra is low in comparison with the results of the SuperTIGER and HEAO-3-C3 experiments, but the data on the isotopic composition still remain unique.

3. "Universal small knee" of cosmic rays

Until the beginning of the new millennium, it was generally believed that, at energies below the Kulikov–Christiansen knee, the energy spectra of cosmic ray nuclei had no significant features other than solar modulation effects below about 20 GeV/nucleon, but feature a universal power-law behavior. Indeed, not a single experiment definitely indicated the presence of such features and/or disagreed with the 'standard CR model.' However, the entire set of data on CR spectra from various experiments could not but cause some concern. Figure 3 shows a compilation of data from all the major proton-spectrum experiments up to the early 2000s, prior to the ATIC experiment (which was the first to directly indicate a violation of the universal power-law behavior of CR spectra below the knee; see Introduction): magnetic spectrometers in Smith et al. [76], Golden et al. [77], LEAP 1987 [78], MASS 1991 [79], IMAX 1992 [80], CAPRICE 1994 [81], BESS 1998 [82], AMS01 1998 [83], CAPRICE 1998 [84]; calorimeters in Proton-3 1966 [85], Proton-3 1966 (Akimov) [86], Ryan et al. 1970 [87], Sokol (1985 r.), Grigorov [88], Sokol 1985 [89]; emulsion balloon experiments in MUBEE (1975–1987) [90], Sanriku (1987 + 1988) [91, 92], JACEE (1979–1994) Takahashi [93], JACEE (1979–1994) Asakimori [94], and RUNJOB (1995–1999) [95]. Although the statistical errors at energies above 1 GeV are large in all the experiments, overall it appears that the entire data set does not fit well into a single power-law spectrum, and the spectrum at energies from about 10 TeV to 100 TeV appears steeper than that between 20 GeV and 10 TeV. The data in the region from approximately 100 GeV to several TeV is scant, so it is difficult to say anything definite about the behavior of the proton spectrum in this range.

The ATIC and CREAM stratospheric spectrometers were the next generation of instruments for direct cosmic ray measurements. Figure 4 shows the magnetic rigidity spectra measured in the experiments ATIC [34], CREAM-I [27], CREAM-III [26] (preliminary results, 2009), CREAM-III [28] (final results, 2017). The spectra measured in the ATIC experiment completely covered the magnetic rigidity range from approximately 30 GV to 30 TV, due to which the previously existing uncertainty range from approximately 100 GV to several TVs was completely filled. At the same time, a feature of the spectrum of protons and helium was

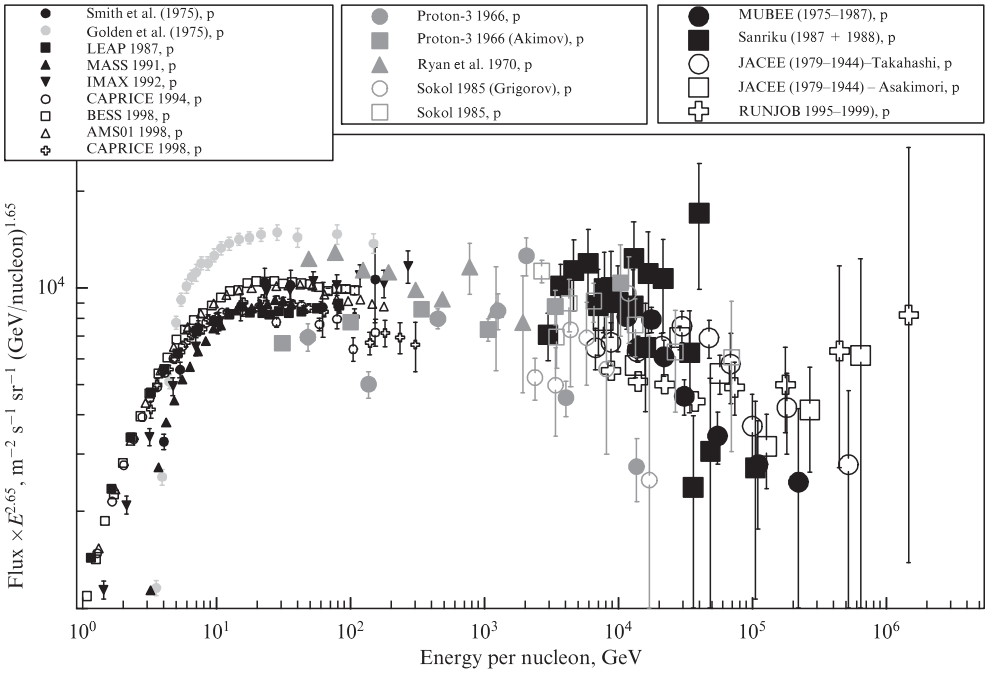

Figure 3. Proton spectrum (energy per nucleon) based on results of direct measurements before the ATIC experiment (early 2000s). Magnetic spectrometers (small icons): Smith et al. [76], Golden et al. [77], LEAP 1987 [78], MASS 1991 [79], IMAX 1992 [80], CAPRICE 1994 [81], BESS 1998 [82], AMS01 1998 [83], CAPRICE 1998 [84]. Calorimeters (medium light icons): Proton-3 1966 [85], Proton-3 1966 (Akimov) [86], Ryan et al. 1970 [87], Sokol (1985) Grigorov [88], Sokol 1985 [89]. Emulsion balloon experiments (large icons): MUBEE (1975–1987) [90], Sanriku (1987 and 1988) [91, 92], JACEE (1979–1994), Takahashi [93], JACEE (1979–1994), Asakimori [94], RUNJOB (1995–1999) [95].

discovered: a significant decrease in the slope of the spectra near a rigidity of several hundred GV (see Fig. 4), which was discussed in Section 1. Another feature of the spectra, which was indicated by the ATIC results, was a sharp kink near a rigidity of 10 TV. However, in this region, the number of ATIC statistics was already small, and the authors of the experiment refrained from interpreting these data as a real indication of the existing kink. The spectra of protons and helium of the CREAM experiment also exhibit a visual indication of kinks in the spectra near the magnetic rigidity of 10 TV. Despite this, it is reported in [27] (CREAM-I) and [26] (CREAM-III, preliminary results) that the spectra of protons and helium are consistent with power-law behavior within the limits of measurement errors. However, the CREAM-III paper [28] finally noted indications of a kink in the spectra near 10 TV, although no estimates of the statistical reliability of the existence of kinks are provided; it was also noted that the data above a possible kink are poorly statistically supported and additional measurements are required. Thus, the ATIC and CREAM experiments together provide a more direct indication of the existence of a knee near a rigidity 10 TV in the spectra of protons and helium than the sum of all the earlier experiments, but ambiguity still remained.

Figure 4 shows that the spectra of protons and helium from the ATIC experiment not only exhibit some signs of a kink near the magnetic rigidity of 10 TV but also showed an overall complex structure, including a deflection in the spectra near the magnetic rigidity of the particles of several hundred GV. A similar deflection was observed in the ATIC spectra of heavy elements [33, 34]. This led V I Zatsepin and N V Sokolskaya, the co-authors of the ATIC experiment, to the hypothesis that these features of the spectra are universal in the sense that they are associated with the presence of

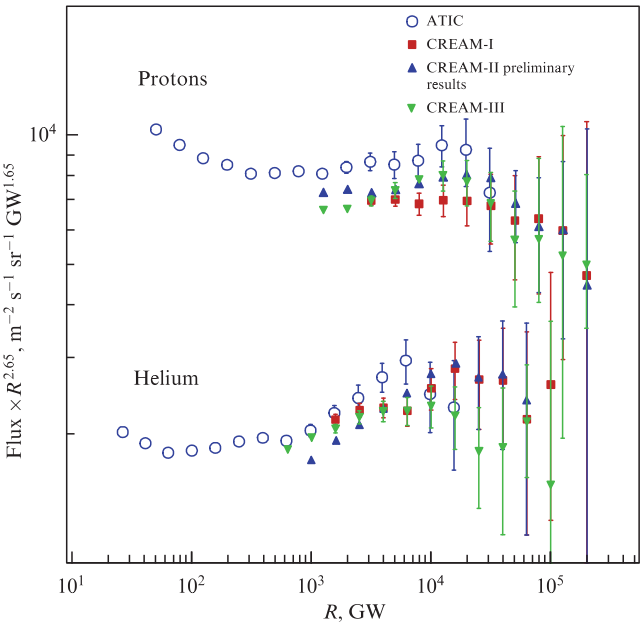

Figure 4. Magnetic-rigidity spectra of protons and helium measured in ATIC [34], CREAM-I [27], CREAM-III Preliminary [26], and CREAM-III [28] experiments.

several types of sources, each of which is characterized by its own spectral exponent of the slope of the power-law spectrum and its own acceleration limit expressed by the maximum magnetic rigidity, the same for all nuclei. Based on this hypothesis, they were able to select three types of sources, which they used to approximate the entire set of experimental data available by 2006 [96]. The resulting approximations are shown in Fig. 5. One of the sources yields a kink in the

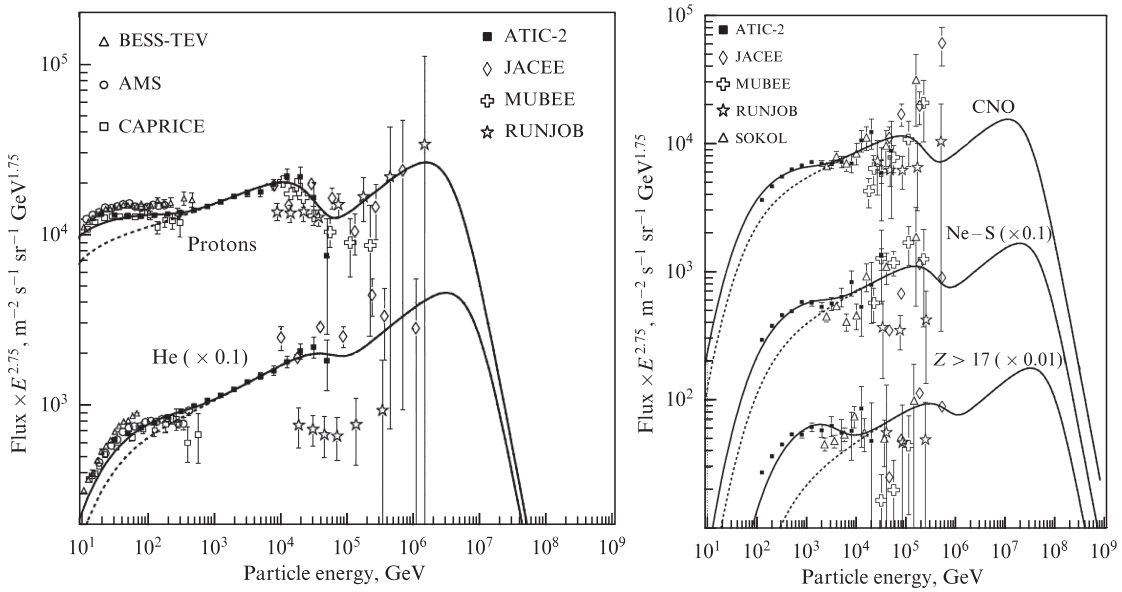

Figure 5. Description of set of experimental data on spectra of cosmic ray nuclei for 2006 using the three-component Zatsepin–Sokolskaya model [96]. (Reproduced from [96] with permission of the authors.) Figure displays data from ATIC experiments [145, 208], BESS-TeV [209], AMS [83], CAPRICE [84], MUBEE [90], JACEE [94], RUNJOB [95], and SOKOL [175].

spectrum of protons near 10 TV and, due to the universality of the cutoff in magnetic rigidity for all nuclei, a similar kink is observed in the spectra of all nuclear groups, including heavy nuclei. Since cutoff occurs for all nuclei at the same magnetic rigidity, the position of the spectral kink, expressed in terms of energy per particle, increases with increasing atomic number of the nucleus. It is of importance to note here that at the time of publication [96] in 2006 there were no experimental indications of a kink in the spectra of heavy nuclei near a magnetic rigidity of 10 TV (which is clearly visible in the right panel of Fig. 5); therefore, the existence of such a 'universal knee' in the spectra of all nuclei, including heavy ones, was a prediction of the three-component Zatsepin–Sokolskaya model to be verified in future experiments.

The first study that directly experimentally confirmed the existence of a universal knee near 1 TV was reported by the NUKLON collaboration in 2017 [97]. In 2018, the NUKLON team published in [98] the first estimates of the statistical reliability of the existence of a kink near 10 TV obtained separately in the spectra of protons, helium, and heavy nuclei and in the rigidity spectrum of all particles. Figure 6 shows the magnetic-rigidity spectra of protons, helium nuclei, heavy nuclei with charges $Z = 6-27$, and the rigidity spectrum of all particles measured by the calorimetric method and the KLEM method in the NUKLON experiment. The ionization-calorimeter method and the KLEM method represent two independent techniques for determining the particle energy in the NUKLON experiment, and it can be seen that both methods provide consistent data regarding the existence of a kink in all of the given spectra near the magnetic rigidity of 10 TV. The number of statistics of the KLEM method are significantly higher than that of the calorimeter; therefore, the KLEM method in the NUCLON experiment is considered the main method that gives physical results, while the calorimeter is used for cross-checking and enhancing the reliability of the data. For the KLEM method, the statistical significance of the existence of a kink in all four spectra shown in Fig. 6 was found to exceed 99.99% (3.9 standard deviations). Actually, the statistical significance was determined by means of rather complex Monte Carlo calculations, and only lower bounds on the statistical significance were obtained because, due to the complexity of the calculations, only a limited number of tests could be applied in the Monte Carlo simulation. Thus, the NUKLON experiment confirmed the existence of a universal knee near the magnetic rigidity of 10 TV in all groups of cosmic rays with a statistical reliability of at least 3.9 standard deviations.

Due to the insufficient statistics from the NUKLON experiment, the position of the kink can only be determined with an accuracy of approximately a factor of two. According to the results of NUKLON [98], taking into account both statistical and methodological uncertainties in processing, the kink lies between 7 TV and 20 TV for all types of nuclei. With such accuracy, this 'small knee' of cosmic rays has a universal character, i.e., for all nuclei, the kink occurs at the same magnetic rigidity, as predicted by the three-component Zatsepin–Sokolskaya model.

At the time of writing this review (winter and spring 2023), the full result of the NUKLON experiment regarding the existence of a universal knee in magnetic rigidity near 10 TV in all groups of nuclei remains the only one, but new experiments provide partial confirmation of it.[1] Verification of the existence of the knee was expected primarily from the DAMPE and CALET experiments.

The DAMPE collaboration began publishing the results of measurements of the spectra of protons [99] and helium [100] in 2017. However, the first preliminary spectra did not extend to a rigidity of 10 TV, so they are irrelevant in what regards the presence of a kink in the spectrum near this rigidity. The most recent data from the DAMPE experiment on the proton spectrum were published in [101], and, on the

[1] Addition made in adjusting the text based on the reviewer's comments: as of October 2023, the situation has not changed. None of the experiments provided results for heavy-nucleus spectra at a magnetic rigidity near 10 TV or higher.

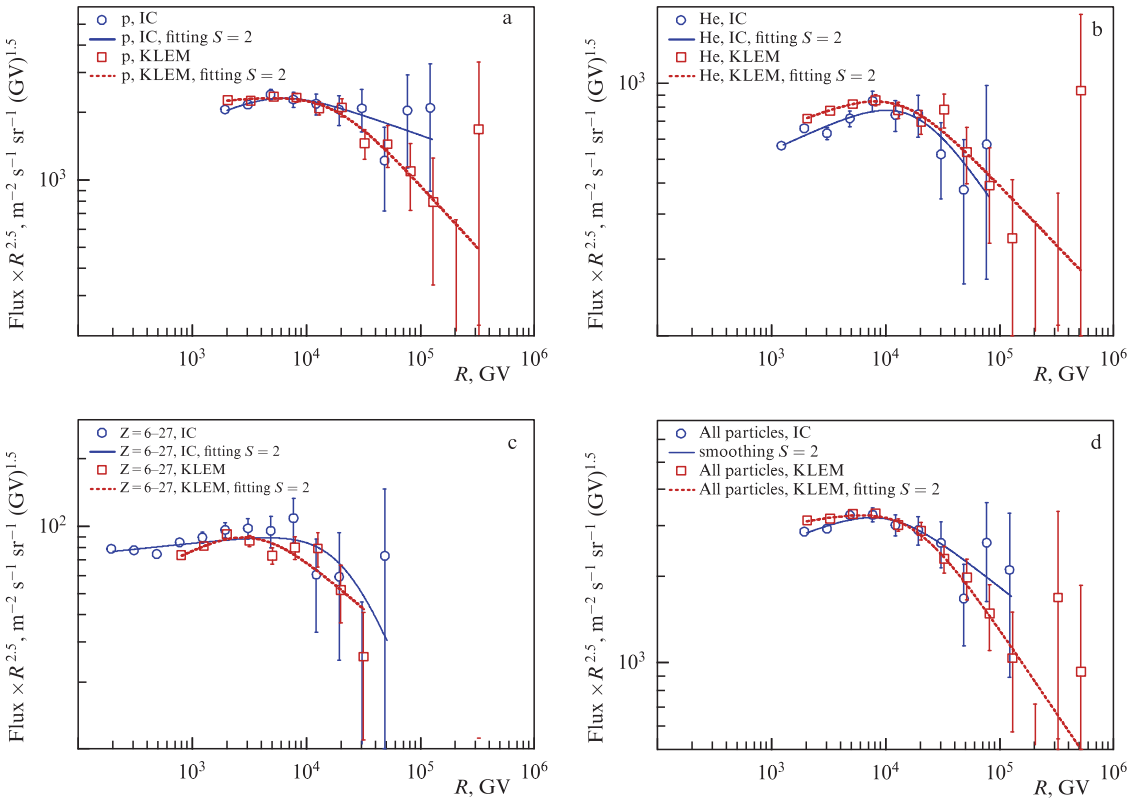

Figure 6. Magnetic-rigidity spectra of protons (a), helium nuclei (b), heavy nuclei with charges $Z = 6-27$ (c), and rigidity spectrum of all particles (d), measured by calorimetric method (IC) and KLEM method in the NUKLON experiment [98]. Fittings of spectra using double power functions are also presented.

spectrum of helium nuclei, in [102]. The spectrum of protons was extended to a magnetic rigidity of about 80 TV, and the spectrum of helium nuclei, to a magnetic rigidity of about 30 TV, while both spectra clearly exhibit a kink between magnetic rigidities of 10 TV and 20 TV. The most recent DAMPE results, together with the proton and helium spectra from the NUKLON experiment, are displayed in Fig. 7. It can be seen that the DAMPE results are in good agreement with the NUKLON results, while the DAMPE spectra of protons and helium clearly indicate the presence of a kink in the spectra between the magnetic rigidities of 10 TV and 20 TV.

The CALET collaboration published preliminary results in 2021 for the proton spectrum in [103] and for the helium spectrum in [104] (see also review [105]). The proton spectrum is extended to a magnetic rigidity of 50 TV and clearly shows a kink near 10 TV, confirming the results of the NUKLON experiment. The helium spectrum has so far been measured up to only 20 TV, so it is too early to make conclusions regarding the presence or absence of kinks in the region from 10 TV to 20 TV, but we can note the good agreement of the CALET helium spectrum with the DAMPE and NUKLON spectra in the region where data overlap. The CALET proton and helium spectra along with the NUKLON and DAMPE spectra are also presented in Fig. 7. Thus, both the new DAMPE and CALET experiments confirm the presence of a kink in the spectra of protons and helium near the magnetic rigidity of 10 TV. It can also be noted that both experiments also confirm the presence of a deflection in the spectra of protons and helium near the magnetic rigidity of several hundred TV, observed earlier in the ATIC, PAMELA, and AMS-02 experiments (see Section 1).

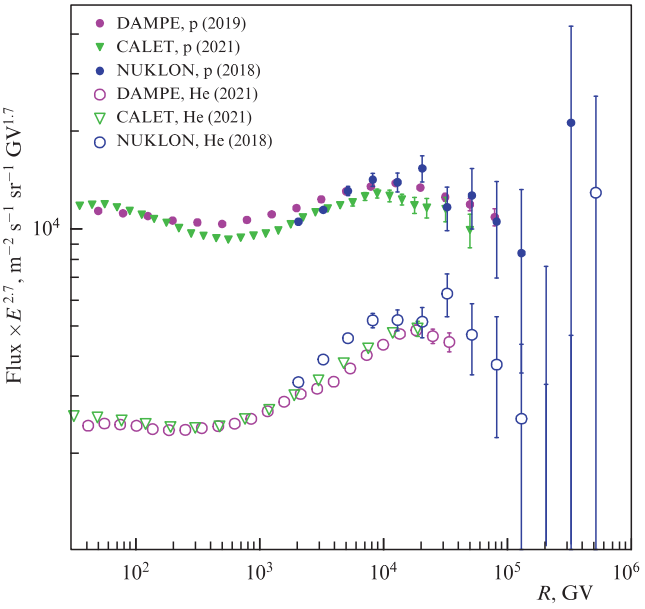

Figure 7. Confirmation of the results of the NUKLON experiment regarding the existence of universal knees in the spectra of protons and helium by the DAMPE and CALET experiments. The experimental points in the figure are presented according to the studies of NUKLON, p (2018) and NUKLON, He (2018) [98]; DAMPE, p (2019) [101]; CALET, p (2021) [103]; DAMPE, He (2021) [102], and CALET, He (2021) [104].

A kink in the spectrum near a magnetic rigidity of 10 TV in the spectra of nuclei heavier than helium has so far been observed in only the NUCLON experiment, since none of the

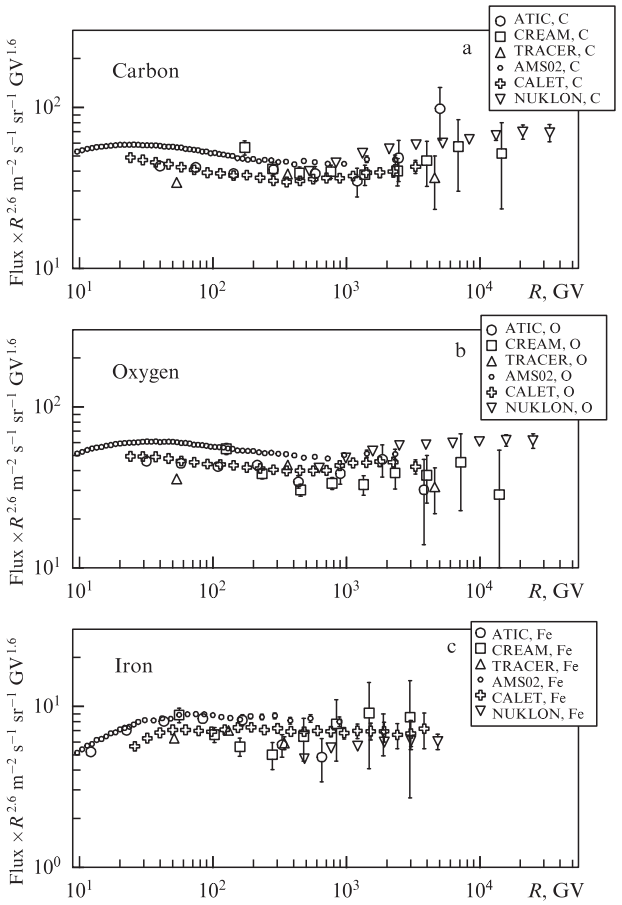

Figure 8. Spectra of magnetic rigidity of carbon (a), oxygen (b), and iron (c) according to modern direct experiments: ATIC C, O, Fe [34]; CREAM C, O, Fe [26, 35, 106]; TRACER C, O, Fe [68]; AMS02 C, O [107]; AMS-02 Fe [108]; CALET C, O [109]; CALET, Fe [110]; NUKLON C, O, Fe [111].

modern direct experiments, except NUCLON, has reached sufficiently high energies in measuring the spectra of heavy nuclei. To increase the number of statistics, the NUCLON experiment combined the rigidity spectrum of all heavy nuclei, but no other experiment has used this approach, so new experiments currently only provide the spectra of individual nuclei. Figure 8 shows the spectra of carbon, oxygen, and iron nuclei according to the direct experiments ATIC [34], CREAM [26, 35, 106], TRACER [68], AMS02 [107, 108], CALET [109, 110], and NUKLON [111]. To plot the spectra in Fig. 8, the original published data, which are usually presented either in terms of energy per particle or in terms of energy per nucleon, were recalculated into magnetic rigidity spectra. It can be seen that it is only the NUKLON experiment that has by now provided statistically supported data for magnetic rigidity above 10 TV for heavy nuclei. The DAMPE collaboration resolves the charge peaks of carbon and oxygen in the cosmic ray spectrum and reports that measurements of the spectra themselves are underway [112], but the results have not yet been published. Thus, verification of the NUKLON result regarding the kink in the spectrum of heavy nuclei remains a matter for the future.

Although the result of the NUKLON experiment regarding a kink in the spectrum of heavy nuclei has not yet been confirmed, indirect confirmation is available from the spectrum of all particles in terms of energy per particle. Already in the article on the three-component model of cosmic-ray spectra [96], a feature was predicted in the form of a bump located between the energy of 10 TeV and 100 TeV in the spectrum of all particles, which is associated with kinks in the rigidity spectra of individual nuclei near 10 TV (Fig. 9a). Since the same magnetic rigidity, depending on the nucleus charge, corresponds to different particle energies, in the spectrum of all particles, plotted in terms of energy per particle, the peaks of different nuclei appear in different places; therefore, the corresponding bump in the spectrum of all particles turns out to be less pronounced than that in the spectrum of each individual nucleus or a bump in the spectrum of all particles, if this spectrum is expressed in terms of magnetic rigidity, as is displayed in Fig. 6d. The presence of a kink in the spectrum of all particles between 10 TeV and 100 TeV energy per particle is clearly visible in the data of the NUKLON experiment [113, 114] and was confirmed in the independent ground-based experiments HAWC [115, 116] and Grapes-3 [117], where the spectrum of all particles was measured using the EAS technique (Fig. 9b).

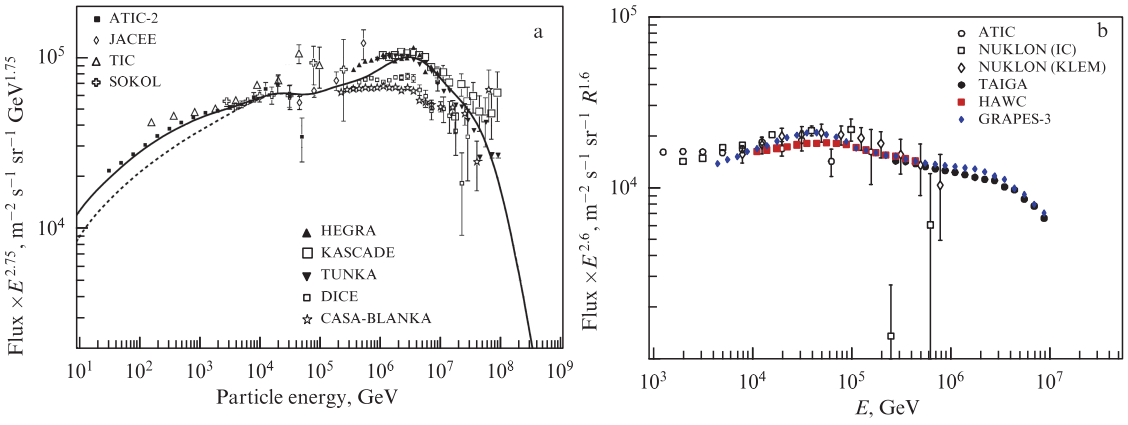

Figure 9. 'Small knee' between energies of 10 TeV and 100 TeV in the spectrum of all particles. (a) Prediction of the small knee by three-component model [96] (published with permission of the authors). Data from experiments ATIC-2 [96], JACEE [93], TIC [210], SOKOL [175], HEGRA [211], KASCADE [212], DICE [213], and CASA-BLANCA [214] are presented. (b) Confirmation of existence of a small knee in modern experiments. Data from ATIC [34], NUKLON (IC), NUKLON (KLEM) [113, 114], TAIGA [36], HAWC [115, 116], and GRAPES-3 [117] experiments are presented.

Although the kink near 10 TV in all nuclear components has been observed so far only in the data from the NUKLON experiment, the first interpretations of this phenomenon have already appeared. It should be noted that observed as a universal feature of the spectra of all nuclei in terms of rigidity is not only a kink near a rigidity of 10 TV but also a deflection in the spectra near a magnetic rigidity of 0.5 TV; therefore, both of these features are interpreted as a manifestation of a single 'bump' in the spectrum, which starts around 0.5 TV and reaches a peak around 10 TV, which is followed by a sharp decline. We refer to this feature of the spectra as a whole as the 10-TV bump.

It is shown in [118, 119] that such a universal bump can be explained by the contribution of a single remnant of a nearby supernova to the observed cosmic ray spectra. For this, incidentally, the explosion of a supernova three thousand years in age with a completely ordinary explosion energy on the order of 10^{51} erg at a distance of 0.16 kpc from Earth is sufficient, assuming that about 10% of the explosion energy is released for the acceleration of cosmic rays. By selecting a suitable limiting energy of cosmic ray acceleration in a supernova remnant, it is possible to approximate with good accuracy the entire available set of experimental data on the kink in spectra near 10 TV (see Figs 3 and 4 in [119]). In [120, 121], the 10-TV bump is also associated with the contribution of a single source in combination with various special models of CR propagation, but nowhere is the analysis developed to the degree of estimating the supernova remnant parameters as in [118, 119]. In [122], the bump is associated with a nearby source, but additionally assumed is the existence of a zone of very low diffusion in the vicinity of the Sun (local bubble).

A completely different idea is proposed in [123, 124]. It is noted that the explanation of only 10-TV bumps, including the universal deflection of the spectra of abundant nuclei near 0.5 TV, from which this bump begins, by a single nearby source contradicts a deflection of about 0.5 TV also being observed in the spectra of fragment nuclei of secondary origin (see Section 5). The spectra of secondary nuclei are determined to a large extent by the interaction of primary nuclei with interstellar gas averaged over the entire Galaxy and the nature of the outflow of primary nuclei into the intergalactic medium from the Galaxy; therefore, the spectra of secondary nuclei should not contain traces of the presence of a nearby local source. Consequently, the 0.5-TV deflection in the spectra of secondary nuclei is not determined by a local source; thus, the 0.5 TV deflection in the spectra of abundant primary nuclei is not associated with a local source either, which implies that the entire 10-TV bump is not associated with a local source. Instead of a single source, the authors of [123, 124] consider the option that the 10-TV bump is a consequence of additional acceleration of cosmic rays on the shock wave of the intense stellar wind of a very close fast-flying star; it is additionally assumed the channeling of cosmic rays from the star to the Earth along the force line of the interstellar magnetic field. A suitable candidate for such an accelerator has been proposed: it is the Epsilon Eridani star located at a distance of 3.2 pc from the Sun. The process of additional acceleration has the same effect on abundant primary nuclei and secondary nuclei, so a deflection near 0.5 TV should be observed in the spectra of all nuclei without exception. At the same time, additional acceleration on the shock wave of a nearby star in model [123, 124] can explain the entire 10-TV bump.

4. Heavy nuclei: dependence of spectra on nuclear charge

4.1 Difference in spectral slopes

The spectra of abundant heavy nuclei (carbon–iron group) of cosmic rays are associated with a number of specific issues that do not yet have clear answers. One of them has already been discussed above in Section 3: is there a universal knee in magnetic rigidity near 10 TV in the spectra of heavy nuclei? Another question is whether the spectra of heavy nuclei feature a universal shape in terms of magnetic rigidity, as should follow from the 'standard model' of cosmic ray physics. One of the particular formulations of the question is: does the slope of the spectra depend on the nucleus charge? The occurrence of such a dependence can in principle be expected from the results of ATIC [25] and subsequent experiments yielding different slopes of the spectra of protons and helium (see Section 1). The dependence of the slope of the spectrum on the nuclear charge for heavy nuclei is then a generalization of the result for protons and helium to heavier nuclei.

As noted in Section 1, the ATIC experiment was the first to make an attempt to answer this question [32]. In the experiment, not just the spectra of heavy nuclei were studied, but, by solving the inverse problem of particle propagation, the spectra of nuclei in the source were calculated based on the experimental spectra, and the slopes of such spectra were compared. To solve the inverse problem, the simplest leaky-box model of cosmic ray propagation (otherwise known as the homogeneous model) was used [125–127]. The propagation model involves some uncertainties; however, it was shown in [32] that, taking into account all the uncertainties, starting from the helium nucleus to the iron nucleus with a reliability of no worse than 3.2 standard deviations, an increase in the steepness of the spectra is observed. From helium to iron, the effective spectral index, when approximating the spectra with power functions for the rigidity range from 50 GV to 1350 GV, increases by approximately 0.25. The achieved statistical significance of the effect is not too great, so the results of ATIC [32] should be checked in new experiments.

The first such significant result was the measurement of the spectrum of the nickel nucleus ($Z = 28$) in the NUKLON experiment [113, 128] (Fig. 10). The nickel nucleus is an even numbered nucleus next to iron. As mentioned above (Section 2), the NUKLON experiment employs two independent methods for measuring particle energy: the calorimetric method (IC in Fig. 10) and the kinematic KLEM method. The IC technique features a lower threshold, but also a lower geometric factor, while the KLEM technique has a higher threshold, but, due to the higher geometric factor, allows the particle flux intensity to be measured up to higher energies; therefore, the entire spectrum of nickel measured in the NUKLON experiment is presented by points of two types: IC and KLEM. In the region of energies (or magnetic rigidity) common to both methods, the results of the methods coincide within the limits of statistical errors. For the studied ranges of magnetic rigidity of iron (40–5000 GV) and nickel (30–1130 GV), it turned out that the spectral index of nickel is 0.19 ± 0.09 greater than that of iron [113, 128]. Although the statistical significance of the difference in spectral indices only slightly exceeds two standard deviations, it is nevertheless indicated that the trend

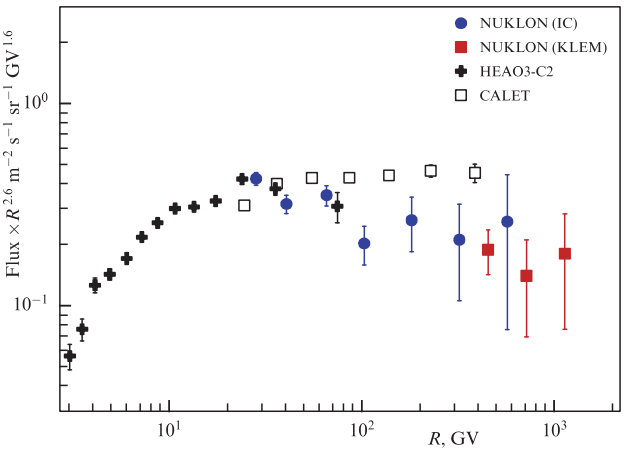

Figure 10. Magnetic rigidity spectra of nickel according to data from various experiments: NUKLON (IC) and NUKLON (KLEM) — points obtained by ionization calorimeter and KLEM technique in NUKLON experiment [113, 128]; HEAO-3-C2 [133]; and CALET [134].

towards an increase in the steepness of the spectra with increasing nuclear charge, discovered in the ATIC experiment [32], continues towards nuclei heavier than iron up to the nickel nucleus. In [113, 128], the conversion of the measured spectra to the source spectrum by solving the inverse propagation problem was not carried out, but the conversion to the source is known to only increase the difference in spectral indices [32].

The NUKLON collaboration has enhanced in [129] the ATIC result [32] by joint the processing of data from the ATIC and NUKLON experiments, also including the nickel spectrum measured in the NUKLON experiment in the processing [113, 128]. In [129], the problem of back propagation of nuclei to search for spectra in a source was solved using the GALPROP[2] system [130, 131], based on solving diffusion equations in the Galaxy, in contrast to the simplified leaky-box approach employed in [32]. Increasing the number of statistics, expanding the energy range, and including the nickel nucleus in the analysis made it possible to enhance the statistical significance of the increase in the steepness of nuclear spectra with increasing charge to 9 standard deviations for the range of magnetic rigidity from 25 GV to 1500 GV.

Although the spectra in sources for nuclei with different charges have not been determined anywhere else but in the ATIC [32] and NUKLON [129] studies, the observed increase in the slope of the spectra with increasing nuclear charge in the observed spectra is consistent with the results of the AMS-02 experiment. In this experiment [132], all nuclei with charges from 2 to 14 were divided into four groups: the most abundant primary nuclei (He, C, O), heavier abundant nuclei (Ne, Mg, Si), nuclei with a high fraction of secondary components (N, Na, Al), and almost purely secondary nuclei (Li, Be, B). In accordance with the results of AMS-02 [132], the slope of the spectra in these groups increases from the first to the last group for the range of magnetic rigidity from 30 GV to 3 TV. In particular, the spectra of the nuclei of the (Ne, Mg, Si) group are steeper than those of the (He, C, O) group, which corresponds to the trend discovered in [32, 129]. We emphasize that converting the spectra of nuclei to the spectra in the source would only increase the difference among the slopes of groups of nuclei reported by AMS-02 [132].

For the four years that passed after the first publication of the NUKLON results for nickel in 2018 [128], these data were the only measurement of the spectrum of nickel up to a magnetic rigidity significantly exceeding 75 GV, which was achieved for nickel in the HEAO-3-C2 experiment as early as 1990 [133]. A new measurement of the spectrum of nickel, in the magnetic rigidity range from approximately 30 GV to 600 GV, was carried out by the CALET experiment and published in 2022 [134] (see Fig. 10). CALET did not find a significant difference between the slopes of the spectra of iron and nickel, thereby not confirming the NUKLON result. Thus, the situation regarding the difference in the slope of the spectra of iron and nickel currently remains unclear; this introduces some new uncertainty into the result presented in [129] regarding the general increase in the slope of the spectra of nuclei with increasing charge. It is noteworthy, however, that the CALET data do not agree well with the data from both HEAO-3-C2 and NUKLON, although the HEAO-3-C2 and NUKLON data virtually coincide in the magnetic rigidity range common to them (see Fig. 10). It should also be noted that, although the spectrum of nickel had never been measured in the high-energy region before the NUKLON experiment, the Ni/Fe flux ratio was measured in the HEAO-3-C3 experiment [135, 136] in the energy range from 10 GeV/nucleon to 500 GeV/nucleon, which, in terms of magnetic rigidity, approximately corresponds to the values achieved in the NUKLON experiment. The Ni/Fe ratio turned out to be decreasing over the entire energy range, and the plots presented in [136] can be used to estimate that this decrease corresponds to a difference in spectral indices of approximately 0.05 (the spectrum of nickel is steeper). Qualitatively, this corresponds to the NUKLON result, although the difference in slopes is smaller (one should not forget about the large statistical errors in both experiments: in particular, in the NUKLON experiment, the difference between the spectral indices of iron and nickel is only slightly larger than two standard deviations). In this controversial situation, new experiments with higher methodological and statistical reliability are needed: both good charge resolution in the iron group and large exposure are necessary.

4.2 Anomaly in the ratio of spectra of C, O, Ne, Mg, and Si nuclei to the spectrum of iron

Another interesting issue regarding the spectra of various heavy nuclei is to what extent the spectra of different nuclei are similar to each other in shape, regardless of the overall steepness of the spectra. The ATIC collaboration was the first to note [137] that the shape of the spectra of abundant heavy nuclei C, O, Ne, Mg, Si differs significantly from that of the iron nucleus, although the spectra of C, O, Ne, Mg, Si themselves are similar to each other. The collaboration presented the ratios of the spectra of C/Fe, O/Fe, (C + N + O + Ne + Mg + Si)/Fe in terms of energy per nucleon to show that all these ratios differ significantly from the horizontal straight line, having the form of a curve with a pronounced minimum near the energy of 30 GeV/nucleon. In other words, the spectrum of iron has a shape that is significantly different from that of other heavy abundant nuclei. In the same ATIC article [137], the deflection in the ratios of the fluxes of abundant nuclei to the iron nucleus was associated with the assumption that all the main sources of cosmic rays in the Galaxy are localized inside individual so-

[2] GALPROP project web site: https://galprop.stanford.edu.

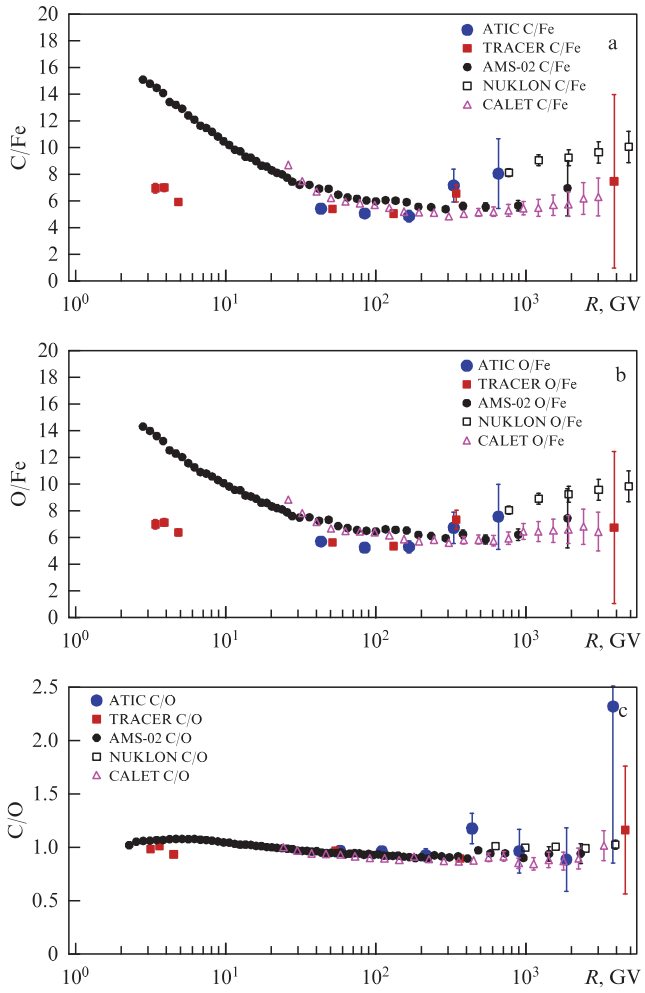

Figure 11. Ratios of fluxes of C/Fe (a), O/Fe (b), C/O (c) nuclei based on data from ATIC experiments [34]; TRACER C, O, Fe [68]; AMS-02 C, O [107], AMS-02, Fe [108]; CALET C, O [109]; CALET, Fe [110]; and NUKLON C, O, Fe [111].

called local bubbles remaining on the site of young star clusters, where an intense star formation once took place and supernovae exploded en masse, with the Sun currently being located inside one of these bubbles. The model predicts deflections in the ratio of the spectra of heavy nuclei to iron, but somewhat smaller than those obtained experimentally in [137].

The issue of the difference between the spectra of heavy nuclei and the spectrum of iron has not been specifically studied since then, but the C/Fe and O/Fe ratios for several experiments can be extracted from the initial data of these experiments for absolute spectra. This procedure was already carried out by the ATIC team [137] for data from the TRACER experiment [68], and the TRACER data confirmed the ATIC results very well. Figure 11 displays the ratios C/Fe, O/Fe, and C/O in terms of magnetic rigidity calculated from the data for the absolute spectra, which are shown in Fig. 8 (ATIC experiments [34]; TRACER C, O, Fe [68]; AMS-02 C, O [107], AMS-02, Fe [108]; CALET C, O [109]; CALET, Fe [110]; NUKLON C, O, Fe [111]). Figure 11 does not display data for the CREAM experiment, since this experiment has very large statistical errors for the spectra of heavy nuclei, and the calculation of ratios, further increasing the errors, yields a statistically insignificant result. Figure 11 shows that all experiments consistently, but with varying degrees of statistical reliability, indicate a deflection in the C/Fe and O/Fe ratios, which occurs in the range from approximately several ten GV to 1 TV (it is still difficult to make more precise conclusions), qualitatively consistent with the ATIC result [137]. In this case, the C/O ratio shown in the same Fig. 11, for all experiments differs slightly from unity, while indicating that the shapes of the spectra of carbon and oxygen are almost the same. Qualitatively, it can be argued that the deflection in the ratio of the spectra of heavy abundant nuclei to the spectrum of iron arises due to the fact that the deflection (levelling) in the absolute spectrum near several hundred GV in the spectrum of iron is much less pronounced than in the spectra of other abundant nuclei if it occurs in iron at all. It should be noted, however, that the quantitative agreement in the nature of the deflection of the C/Fe and O/Fe ratios among different experiments is not very good, which indicates the need for new experiments with high methodological and statistical reliability of the data. To our knowledge, the reason for the deflection of the C/Fe and O/Fe ratios has not been discussed anywhere else but in the original ATIC paper [137].

5. Secondary nuclei

Fluxes of secondary nuclei are known to be the basis for determining the parameters of cosmic ray propagation models [126, p. 599], [7, p. 219], [138, pp. 56–63]. It is usually assumed that the nuclei of lithium, beryllium, and boron are purely secondary [139–142], i.e., that they are products of the fission of primary nuclei accelerated in cosmic ray sources during interaction with interstellar gas (mainly hydrogen and helium) on the way through the Galaxy. Among these nuclei, the boron nucleus is the most widely used, since the spectra of lithium and beryllium are much more difficult to measure. There is an option that, although these nuclei are secondary, a certain number of such nuclear fragments already appear during the acceleration of cosmic rays in supernova remnants; therefore, such secondary nuclei themselves participate in the acceleration process [143]. If secondary nuclei appear only on the path of primary nuclei through the Galaxy, it should be expected that the ratio of the flux of a secondary nucleus to that of the primary nucleus of which it is a fragment (for example, B/C) is described by a curve that decreases with increasing nuclear energy (or magnetic rigidity). If, however, secondary nuclei appear in significant quantities already in supernova remnants and can themselves participate in acceleration, models [143] predict that, at energies above 1000 GeV/nucleon (magnetic rigidity 2000 GV), the ratio can again go up.

Figure 12 shows the B/C ratios in terms of energy per nucleon measured in the experiments of AMS-02 [144], ATIC [145], CREAM [146], PAMELA [147], TRACER [148], NUKLON (KLEM technique) [97], DAMPE [149], and CALET [150]. At energies significantly higher than 1000 GeV/nucleon, data are reported by the NUKLON and TRACER experiments alone. Both of these experiments indicate a leveling of the ratio at energies above 1000 GeV/nucleon, or even a change with energy from a decrease to an increase in the ratio, but the statistical errors of both experiments in this area are large, so confident conclusions about the nature of the ratio at high energies cannot yet be made. Thus, the model with additional acceleration of secondary nuclei in supernova remnants [143] does not disagree with experiment, but does not yet

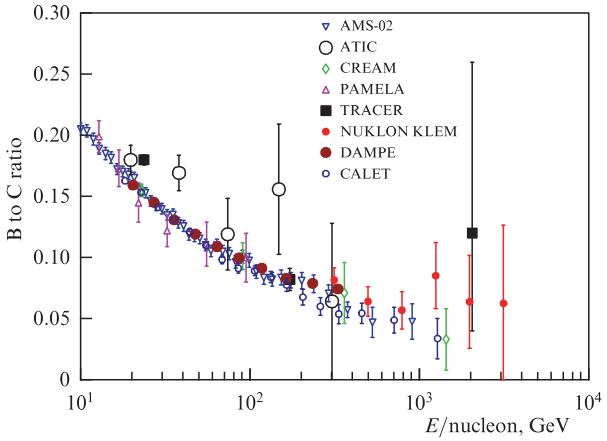

Figure 12. Ratio of B/C fluxes as a function of energy per nucleon. Data from AMS-02 [144], ATIC [145], CREAM [146], PAMELA [147], TRACER [148], NUKLON [97], DAMPE [149], and CALET [150] experiments are displayed.

have clear confirmation. New data are needed at higher energies with higher statistical confidence.

The data on the B/C ratio obtained in the AMS-02 experiment are currently more recent than those published in [144]. These results were presented in a 2021 review [107] (Fig. 13a), but the B/C ratio is given in terms of magnetic rigidity, due to which they cannot be directly compared with the data from previous experiments, which are displayed in Fig. 12. However, these latest results of AMS-02, differing from previous results in detail, extend to a magnetic rigidity of up to 2 TV, which corresponds to an approximate energy of 1 GeV/nucleon, i.e., do not provide information about the behavior of the ratio at significantly higher energies, where signs of additional acceleration of secondary nuclei in supernova remnants are expected in the ratio of secondary nuclei to primary ones.

For not too high nuclear energies (less than 1 TeV/nucleon or magnetic rigidity less than 3 TV), the AMS-02 experiment currently provides the most precise data on the ratio of fluxes of secondary to primary nuclei. The high statistical reliability of the results made it possible to discover a new phenomenon: the AMS-02 data definitely indicate the presence of spectral deflections near the magnetic rigidity $\rho_{\text{br}} = 200$ GV not only in the spectra of abundant primary nuclei (see Section 1) but also in the spectra of secondary nuclei Li, Be, and B [107, 132]. Moreover, the deflection in the spectra of secondary nuclei turned out to be stronger than that in the spectra of primary nuclei. This is best seen in the ratios Li/C, Be/C, B/C, Li/O, Be/O, and B/O (see Fig. 13). Figure 13 shows that the ratios themselves exhibit a deflection, which indicates that the deflection of secondary nuclei is stronger than that in the spectra of carbon and oxygen. The significance of the detected effect exceeds 5σ.

The deflection in the spectra of cosmic ray nuclei near ρ_{br} is discussed in many publications, including [20, 151]. Several more references to this problem can be found in [151]. In [20], based on numerical modeling in the GALPROP system, ten models of the propagation and origin of cosmic rays (different propagation modes, different types of source spectra, local and distributed sources) are analyzed. The data provided by this modeling enable making some preliminary hypotheses to explain the discussed effect. A stronger deflection in the spectrum of secondary nuclei near ρ_{br} than that in the spectra of primary nuclei may imply a change in the behavior of the diffusion coefficient near this point (a decrease in the spectral index of the power-law dependence of the diffusion coefficient on the magnetic rigidity of nuclei). At the same time, if the ρ_{br} deflection in the spectra of primary nuclei is explained by the corresponding deflection in the primary spectrum of distributed sources, the deflection in the spectrum of primary and secondary nuclei should be exactly the same (the shape of the secondary spectra differs from that of the primary spectra by only a smooth power factor of the magnetic rigidity [151]); therefore, there will be no deflection in the B/C type ratios. If the deflection in the primary nuclei is only explained by the contribution of a local source, and there is no deflection in the spectrum of a distributed source, there will be no deflection at all in the spectrum of secondary nuclei [123, 124]. In this case, in the ratio of secondary nuclei to primary ones, one can expect not a deflection near ρ_{br} but, on the contrary, a kink, which is clearly not observed. Moreover, since the nearby source supplies carbon at high energies, but not secondary boron nuclei, at high energies (above ρ_{br}) an additional downward bend can be expected in the B/C ratio [151], which disagrees with observations. This conclusion should be valid not only for B/C but for any ratio of secondary to primary nuclei. Thus, the deflection in the ratio of secondary

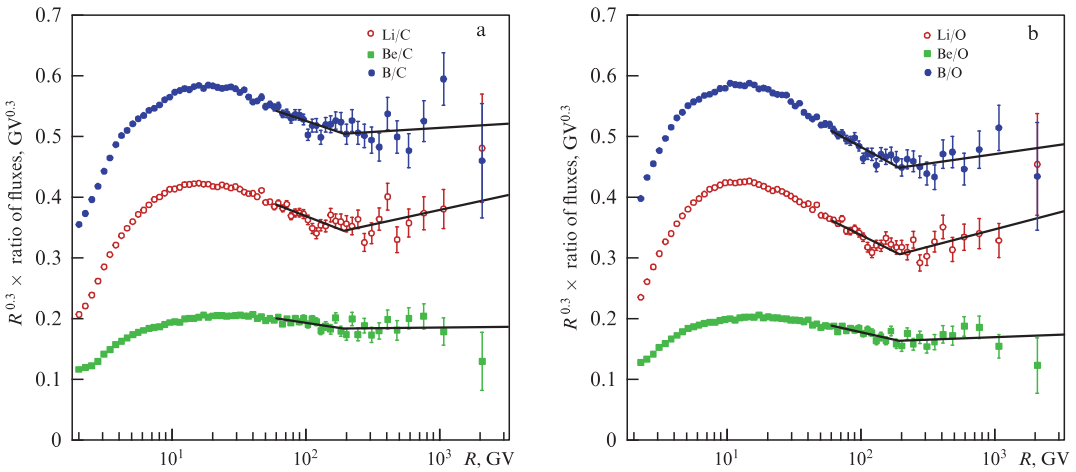

Figure 13. (a) Ratio of Li, Be, B fluxes to flux of carbon and (b) to flux of oxygen according to data from AMS-02 experiment [107, 132]. Figure also shows piece-wise exponential fitting of ratios based on the same data [107, 132].

nuclei to primary ones, discovered by AMS-02 [107, 132], rather indicates a deflection in the dependence of the diffusion coefficient on the magnetic rigidity near ρ_{br}, but this issue is still very far from being clear. It is possible, incidentally, that what is observed is a combination of several different reasons, including effects associated with the diffusion coefficient, effects of additional acceleration by the shock wave of a nearby star [123, 124], and, possibly, some other mechanism. Further progress requires, at least, confirmation of the AMS-02 results in independent experiments.

6. Problem of the ratio of sub-iron to iron and spectra of low-abundance nuclei

As already noted in Section 2, one of the tasks of the HEAO-3-C3 experiment (HNE), which carried out measurements back in 1979–1981, was a detailed measurement of the ratio of the spectra of $Z = 18$–28 nuclei to the spectrum of the iron nucleus. These data are presented in [135, 136, 152, 153]. Displayed in these papers are the spectra for the nuclei Ar, K, Ca, Sc, Ti, V, and Cr with respect to iron. It is assumed that the nuclei K, Sc, Ti, V, and Cr are almost purely secondary; therefore, for them, falling ratios of the spectra to the spectrum of iron can be expected. The spectra of these nuclei were measured in the HEAO-3-C3 experiment in the energy range from approximately 10 GeV/nucleon to 100–180 GeV/nucleon (the upper limit depends on the nucleus), and yielded the expected drop in intensities. For the Ar and Ca nuclei, it is expected that they are partly primary and partly secondary, and, for them, one would expect a falling ratio of the spectrum to the iron spectrum, gradually reaching a plateau. However, HEAO-3-C3 results turned out to be different. Instead of reaching the expected plateau, above energies of 200 GeV/nucleon a sharp increase in the Ar/Fe and Ca/Fe ratios is observed, which continues to energies of approximately 600 GeV/nucleon. This result is presented chronologically in the first three publications [135, 136, 152] on this issue. In the latest paper [153], the results of the previous three papers were refined using more recent nuclear fragmentation cross sections. It is noted that the results have remained almost unchanged, but, in the last paper, the spectra of Ar and Ca are only presented up to energies of 119 and 112 GeV/nucleon, respectively, so the behavior of the ratios after 200 GeV/nucleon is not seen. This weird effect is discussed in [152]: the authors failed to conclude with certainty whether it is methodological or a real effect. The problem was that the technique used to determine the particle energy, based on measuring the ionization loss density, does not itself distinguish between very low and very high energy nuclei, so the high energy part of the ratios of argon and calcium to iron fluxes could be distorted by incorrectly interpreted events associated with low energy nuclei. The HEAO-3-C3 experiment did not involve an independent technique for selecting low-energy nuclei. The intensity ratios of the Ar/Fe, Ca/Fe, and Ti/Fe spectra measured in the HEAO-3-C3 experiment (HNE), according to the data from 1988 [152] and 1989 [153] studies (the data of these two publications are identical), are displayed in Fig. 14a.

The ATIC experiment had to verify the results of the HEAO-3-C3 experiment. The charge resolution of the ATIC experiment in the S–Cr region ($Z = 16-24$) is not very good, so the first target of the study was the ratio of titanium to iron, since the charge line of titanium is better distinguished than the other nuclei in this group. Figure 14b displays the Ti/Fe ratios measured in the HEAO-3-C3 [152, 153] and ATIC [154] experiments. The HEAO-3-C3 and ATIC results are in very good agreement up to an energy of 100 GeV/nucleon, but the two HEAO-3-C3 points in the region of 100–200 GeV/nucleon are a continuation of the falling curve, while the two ATIC points, up to an energy of 400 GeV/nucleon, sharply go up, similar to the Ca/F and Ar/Fe ratios in the HEAO-3-C3 experiment. Due to the limited statistics of the ATIC experiment data at energies above 100 GeV/nucleon, the authors of [154] were unable to draw a definite conclusion about the reality of the observed effect. There is an urgent need to improve the statistics for determining the ratios of sub-iron nuclei ($Z = 16-24$) to iron for energies above 100 GeV/nucleon.

To increase the statistical significance of the result, the ATIC collaboration determined in [137] the ratio of fluxes, not of individual nuclei to an iron nucleus but of the entire total spectrum for nuclei from $Z = 16$ to $Z = 24$ in terms of energy per nucleon. The resulting ratio again exhibits an increase at high energies, this growth starting at approximately 50 GeV/nucleon (Fig. 15a). The statistical significance of the existence of a kink in the ratio was found to be 0.997 (about 3σ). It was also shown that a kink in the ratio of the fluxes of sub-iron nuclei to iron exists separately for the group of charges from 16 to 20 and from 21 to 24 (see Fig. 4 in [137]). It can be considered an indication that this kink is universal for all, at least even, nuclei of the sub-iron group ($Z = 16-24$).

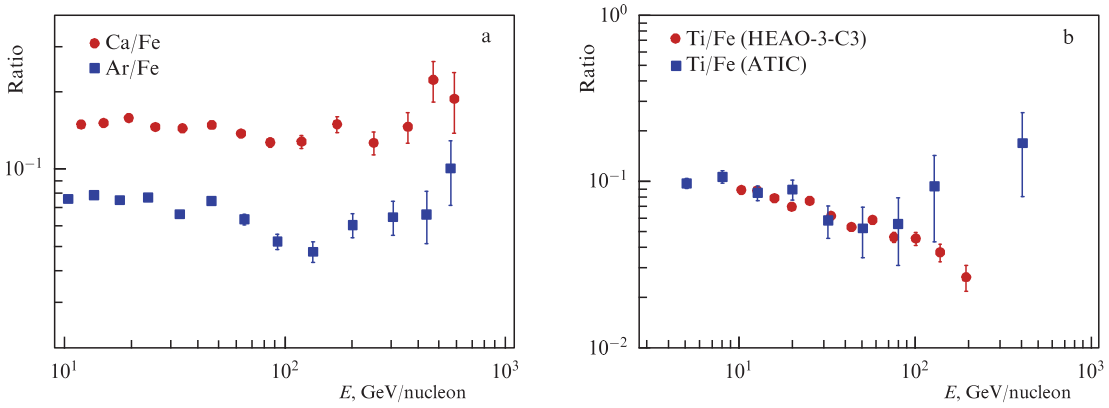

Figure 14. (a) Intensity ratios of Ar/Fe and Ca/Fe spectra according to HEAO-3-C3 experiment [152, 153]. (b) Ti/Fe ratios measured in HEAO-3-C3 [152, 153] and ATIC [154] experiments.

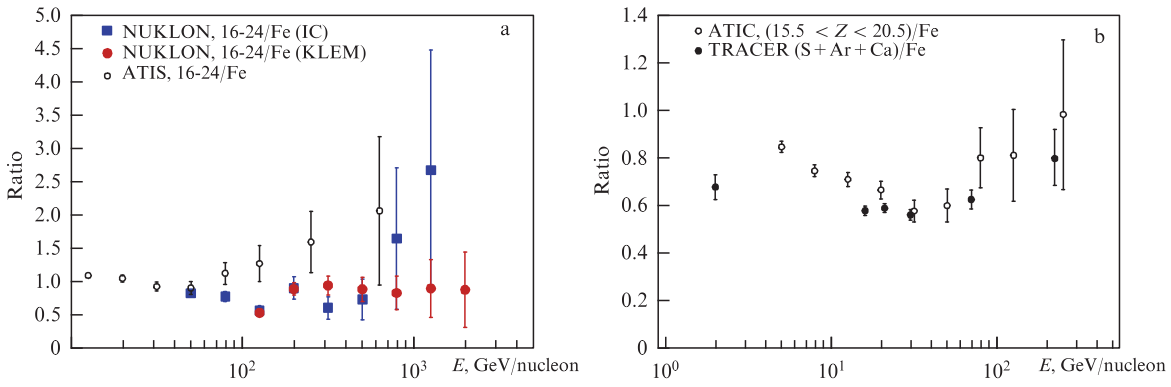

Figure 15. (a) Ratio of total flux of nuclei from $Z = 16$ to $Z = 24$ to flux of iron [137] as a function of energy per nucleon and similar data from NUKLON experiment [98] for two methods for determining energy — calorimetric and KLEM. (b) Ratio (S + Ar + Ca)/Fe according to data from TRACER experiment [67] and ratio $(15.5 < Z < 20.5)$/Fe according to data from ATIC experiment [137].

In no experiment other than ATIC were the ratios of the fluxes of groups of sub-iron nuclei to iron compared, so the ATIC results [137], strictly speaking, had nothing to be compared with. However, according to the TRACER experiment [67], the ratio $(S + Ar + Ca)/Fe$ can be calculated, which should differ from the ratio $(15.5 < Z < 20.5)/Fe$ only by the contribution of odd nuclei, which is small. Therefore, these two ratios can be compared, which was done in [137] (Fig. 15b). It can be seen that the ATIC and TRACER data are in good agreement with each other in the energy range from 30 to 300 GeV/nucleon (TRACER points are slightly lower, as expected), demonstrating a deflection near 40–50 GeV/nucleon, although the statistical reliability of the data from both experiments is not high.

The ratio of the total flux of nuclei from $Z = 16$ to $Z = 24$ to the iron nucleus was measured in the NUKLON experiment [98] (Fig. 15a). These results can be compared with the ATIC result directly. The NUKLON data obtained using the two different techniques for energy determination implemented in this experiment consistently indicate a deflection near 130 GeV/nucleon, which is more similar to the position of the deflection in the HEAO-3-C3 data than in ATIC (about 50 GeV/nucleon). After the deflection, the data provided by different NUKLON methods differ, although within the limits of statistical error. The calorimeter data show a rapid increase in the ratio (but the statistical errors are very large), while the KLEM method data are better statistically supported, but do not exhibit a steep increase, although they do not indicate a drop in the ratio. Most likely, after a slight increase, a plateau is observed.

In [137], an explanation was proposed for the deflection in the ratios of sub-iron group nuclei to iron in the same local bubble model in which the deflections in the ratios of abundant even nuclei to the iron nucleus were explained (see Section 4.2). The local bubble model, in principle, predicts both of these phenomena. However, the model somewhat underestimated the degree of deflection in the sub-iron-to-iron ratios in the ATIC data [137], although in the NUKLON data [98] the deflection is weaker and better fits the model. Thus, the degree of agreement of the local bubble model with experimental data currently remains in question due to the uncertainty of the experimental data themselves.

The data from all the experiments considered, HEAO-3-C3, ATIC, TRACER, and NUKLON, consistently indicate that, in the ratio of fluxes of sub-iron nuclei to iron, no expected drop in the ratio with increasing energy occurs; rather, there is an indication of an increase in this ratio. There is no quantitative agreement in the data from different experiments, but there is qualitative agreement in the behavior of the ratio at high energies. Apparently, continuation of the experimental study of this phenomenon in more methodologically reliable and statistically supported experiments is required.

All sub-iron region nuclei are expected to contain a significant admixture of secondary nuclei (and some are predominantly secondary). Another way to obtain a group of nuclei that may have a significant proportion of secondary ones is to specifically consider low-abundance odd nuclei. Based on the NUKLON experiment data, the ratio of the total flux of odd nuclei 9, 11, 13, 15, 17, and 19 to the total flux of even nuclei 10, 12, 14, 16, 18, and 20 was determined in [129]. All nuclei are taken from the same charge range $Z = 9-20$. The expected behavior of the ratio of odd nuclei to abundant even nuclei of the same charge range is a drop in the ratio with increasing energy, due to the significant fraction of the secondary component in the low-abundance odd nuclei. The NUKLON data exhibit the opposite trend (Fig. 16a). The nuclear spectra were obtained as a result of a deconvolution procedure, due to which neighboring points in the spectra are correlated, so the errors do not reflect statistically independent errors of each point of the curve separately but, to a large extent, uncertainties in the behavior of the curve as a whole. In this situation, the statistical significance of the presence of a growth of the ratio can only be determined by a full Monte Carlo simulation of the entire process of data processing. This method was used to determine the uncertainties in the average integral spectral index of odd and even nuclei for various magnetic rigidity thresholds [129]. Figure 16b shows the statistical distributions obtained by the Monte Carlo method for the determined values of the mentioned spectral indices of odd and even nuclei for a threshold of 400 GV. Curves displayed in Fig. 16 correspond to a difference in spectral indices of 3.4 standard deviations, i.e., a strong indication was obtained that the spectra of odd nuclei are flatter than those of even nuclei for the magnetic rigidity of both above 400 GV. Apparently, the effect requires further study to obtain a higher statistical significance of the result.

Summarizing, the increase in the ratio of fluxes of sub-iron to iron nuclei at high energies and the increase in the ratio of low-abundance odd nuclei to abundant even nuclei at a magnetic rigidity above 400 GV disagree with naive expecta-

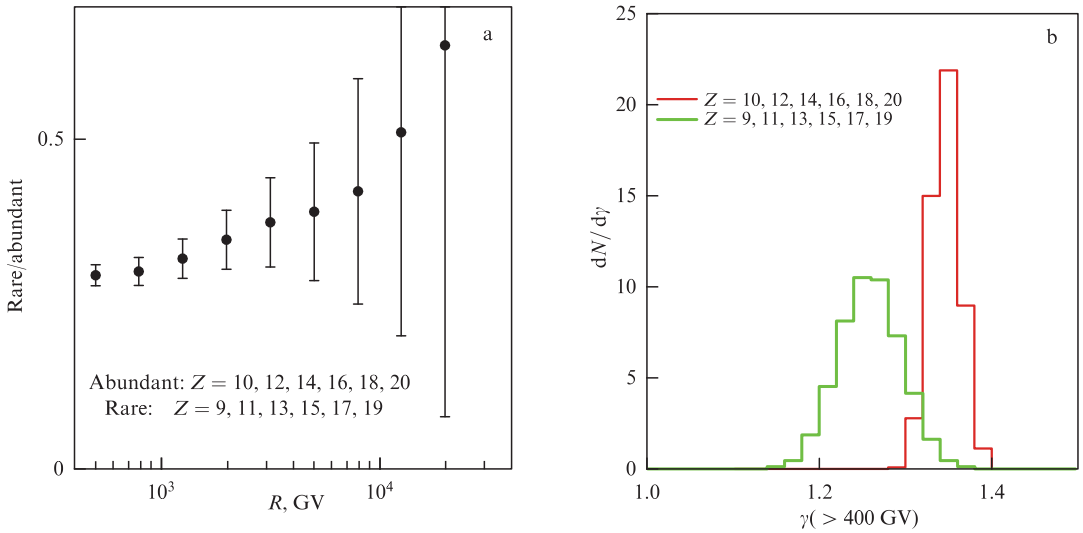

Figure 16. (a) Ratio of total flux of odd nuclei 9, 11, 13, 15, 17, 19 to total flux of even nuclei 10, 12, 14, 16, 18, 20 according to NUKLON experiment [129]. (b) Distribution of spectral indices of integral spectra of odd and even nuclei above magnetic rigidity threshold of 400 GV obtained by the Monte Carlo method to determine errors of spectral indices and statistical reliability of the conclusion that spectra of odd nuclei are flatter than those of even nuclei.

tions based on simple classical models of cosmic ray propagation. They look like related phenomena and may well turn out to be so. However, the nature of these phenomena remains enigmatic, and experimental results require verification and enhanced reliability.

7. Superheavy nuclei and isotopic composition of cosmic-ray nuclei

Referred to as superheavy cosmic-ray nuclei are nuclei heavier than iron, usually starting with zinc ($Z = 30$) [155]. The fluxes of such nuclei are very small compared to those of nuclei from protons up to iron; therefore, in experiments, due to a lack of statistics, their energy spectra are usually not measured, but only fluxes above a certain detection threshold are determined (however, there are exceptions to this rule, for example [156, 157]). The elements between iron and zinc occupy to some extent an intermediate position between heavy and superheavy nuclei, featuring relatively high flux intensities. In particular, for the nickel nucleus, as already mentioned in Section 4.1, in the HEAO-3-C3, NUKLON, and CALET experiments, the spectrum could be measured up to energies above several hundred GeV per nucleon.

Figure 17 shows basic data on the elemental composition of superheavy cosmic-ray nuclei normalized to the flux of iron nuclei (iron flux is taken as unity) based on the results of the HEAO-3-C3 [155], SuperTiger [158], ACE-CRIS [159], and LDEF [72] experiments. For comparison with experimental data, the plots show the elemental composition of the solar system [160].

In the upper-left panel of Fig. 17, blue circles represent the results of the HEAO-3-C3 experiment, which measured the charge composition of superheavy nuclei. Although the HEAO-3-C3 experiment was carried out from 1979 to 1981 (a total of 454 days of collecting statistics, exposure of 6 m^2 sr years), its results are still of importance, since to this day this experiment has record statistics for nuclei in the range from $Z = 33$ to $Z = 69$. The HEAO-3-C3 results [155] are based on a technique that implements a certain compromise between the quality of the charge resolution and the number of statistics. Results are presented for charges ranging from 33 to 82 and, in the main group of data, for charges from 33 to 60. Charges are resolved for pairs of two neighboring nuclei, one of which is odd and the other even: 33 + 34, 35 + 36, etc. For charges above 60, the HEAO-3-C3 experiment does not resolve neighboring charge pairs, and the results reported in [155] are only presented for a few broad charge groups. Figure 17 does not show such data. Several references to previous studies of the HEAO- 3-C3 are contained in [155], where priority in processing was given to high charge resolution at the expense of statistics. Along with the HEAO-3-C3 data, Figure 17 displays data from the SuperTIGER [158] and ACE-CRIS [159] experiments. These two experiments provide data with element-by-element resolution; therefore, for comparison with the results of HEAO-3-C3, the results were summed over pairs of odd and even nuclei (33 + 34, 35 + 36, 37 + 38, and 39 + 40). It is clearly seen that the statistical confidence in the data from the HEAO-3-C3 experiment is better than that of more recent experiments, SuperTIGER and ACE-CRIS. Indeed, of the modern experiments in the range of nuclear charges up to 60, the greatest number of statistics are provided by the SuperTIGER experiment with an exposure of 0.6 m^2 sr years, i.e., approximately an order of magnitude smaller than that of HEAO-3-C3, with a smaller range of measured charges for superheavy nuclei (the entire charge range of SuperTIGER was $14 \leqslant Z \leqslant 40$). Thus, over the past decades since the HEAO-3-C3 flight, the technique of direct observations of superheavy nuclei has advanced only in the direction of improving charge resolution (the charge resolution of SuperTIGER, determined from the iron peak, was 0.18 charge units), but not in the direction of increasing the number of statistics.

Figure 17b presents the results of the SuperTIGER and ACE-CRIS spectrometers with element-by-element charge resolution, natural for these experiments, for the nuclear charge range of $30 \leqslant Z \leqslant 40$. The data from both experiments are in agreement with each other within statistical errors, with the exception of the content of yttrium nuclei ($Z = 39$).

Most data on the chemical composition of cosmic rays for $Z \geqslant 70$ charges is currently provided by the LDEF space

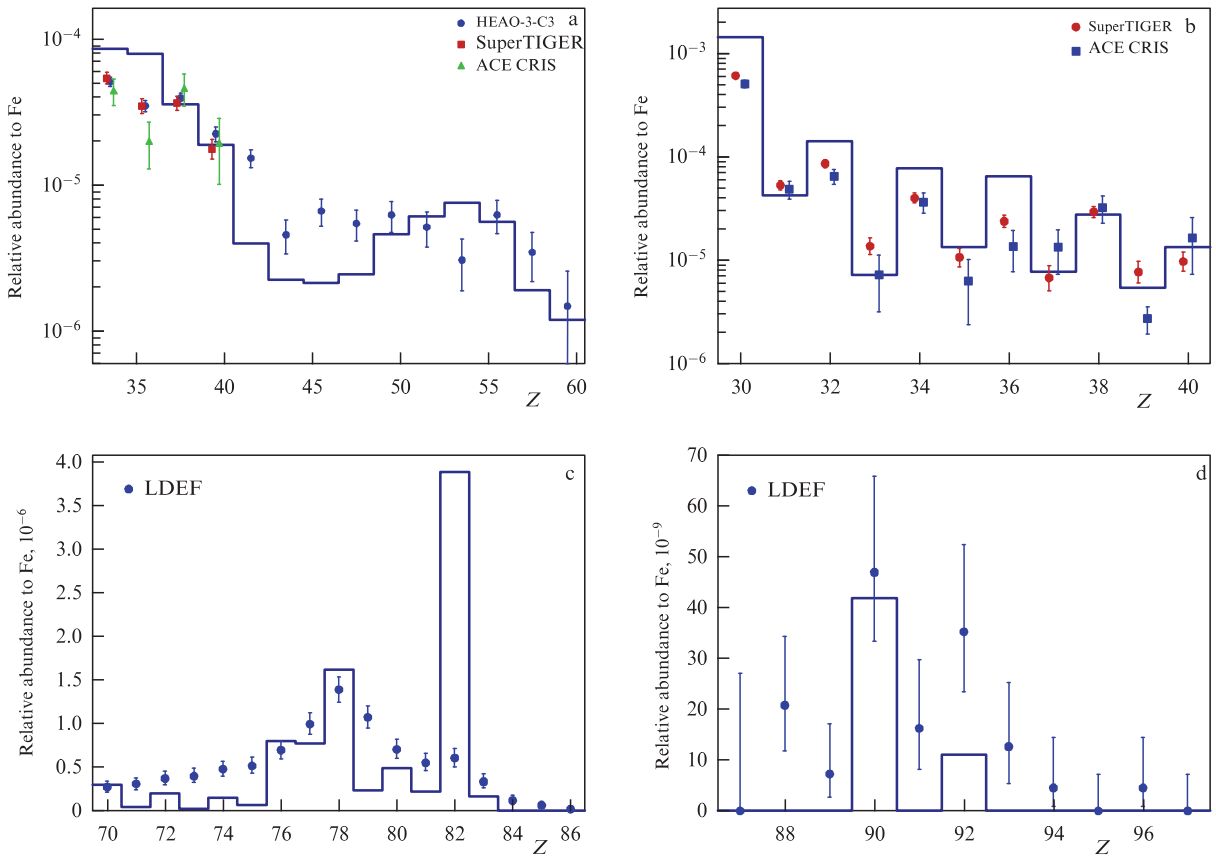

Figure 17. Elemental composition of superheavy nuclei of cosmic rays normalized to flux of iron nuclei according to data from HEAO-3-C3 [155], SuperTiger [158], ACE-CRIS [159], and LDEF [72] experiments. Histograms on plots show elemental composition of the solar system [160].

experiment, based on the use of solid-state track detectors (see details in Section 2). The immense exposure of this instrument (170 m^2 sr years; see Section 2) made it possible to obtain statistics up to trans-uranium elements. The results of this experiment are displayed in Fig. 17c, d. In contrast to the original LDEF publication [72], where all data, including the chemical composition of the solar system, are presented as the ratio of the abundance of a certain nucleus to the total integral over the entire charge region $Z \geqslant 70$, in plotting Fig. 17, for ease of perception and comparison, the composition was recalculated into normalization to iron content, as in Fig. 17a, b.

The physics explored in experiments on the chemical composition of superheavy cosmic-ray nuclei is associated with the examination of the share of s- and r-processes in the synthesis of superheavy nuclei, with signatures of nuclear acceleration in the standard interstellar medium (ISM), or in the stellar wind material of heavy Wolf–Rayet stars in OB associations (Massive Star Material, MSM), and in the differences in the efficiency and acceleration mechanisms of refractory and volatile elements [161]. It is noted that superheavy nuclei are a sensitive indicator of the mechanisms of cosmic ray propagation, since the cross section of their inelastic scattering on atoms of interstellar gas is large, and that the fluxes of superheavy nuclei, due to their short paths to nuclear interaction, are sensitive to the immediate solar environment in the Galaxy, in contrast to lighter cosmic-ray nuclei. All these problems are actively discussed in the quoted articles on experiments on superheavy nuclei [72, 155, 158, 159].

Based on a comparison of the abundances of superheavy elements observed in cosmic rays with those predicted for the chemical composition of the stellar wind of heavy stars [162] and for the ordinary interstellar medium, for which the chemical composition of the solar system is used [160], the SuperTIGER experiment concludes that the composition of CRs corresponds to 19^{+11}_{-6} % MSM and ~ 81% ISM [158]; the ACE-CRIS experiment reports figures of approximately 20% MSM and 80% ISM (no errors presented). This indicates a reasonable agreement between the experiments. These values imply that supernova explosions, leading to the acceleration of cosmic rays, occur predominantly within OB associations containing many young supermassive stars. The SuperTiger and ACE-CRIS experiments also agree in the estimate that refractory elements are accelerated 4–4.5 times better than volatile ones, while the contents of both, compared to the concentrations of elements in the solar system, grow linearly according to the same law with an increase in nucleus mass.

In analyzing data from the LDEF experiment [72], special attention was paid to the signatures of the r- and s-processes in the synthesis of superheavy elements. It is usually believed that predominantly responsible for the synthesis of elements of the platinum group ($74 \leqslant Z \leqslant 80$) are r-processes, while for the lead group ($71 \leqslant Z \leqslant 73$), s-processes (together they constitute the so-called double r–s peak in the abundance of elements). Moreover, according to the LDEF results [72], the Pb/Pt ratio in cosmic rays is significantly lower than in the solar system. This phenomenon represents a certain enigma, since, for the two other double r–s peaks, with lower charges, nothing similar is observed.

It should be noted that the composition of cosmic-ray nuclei for charges from $Z = 41$ to $Z = 69$ was last studied in

the HEAO-3-C3 experiment, which operated from 1979 to 1981, with low charge resolution. There is a glaring lack of experimental data for this charge range.

Among all the experiments, a special role is played by the ACE-CRIS mission, which is still operating, since all the above-mentioned space and stratospheric experiments HEAO-3-C3, SuperTIGER, and LDEF were carried out inside Earth's magnetosphere, which significantly modifies the fluxes of nuclei with a magnetic rigidity of less than the few GVs primarily recorded in these experiments. However, ACE-CRIS operates at the solar-terrestrial Lagrange point L1, outside Earth's magnetosphere, where nuclear fluxes are only affected by solar modulation. Therefore, despite the relatively low number of statistics from the ACE-CRIS experiment, its data are important for the physics of superheavy-nucleus CRs. It can be noted that there are no particular disagreements among the results of various modern heavy-nucleus experiments, with the exception of the above-mentioned case of the yttrium nucleus in the ACE-CRIS and SuperTIGER experiments.

The ACE-CRIS experiment is also of interest, since it can determine not only the charge composition of cosmic rays but also the isotopic composition of individual elements. In this experiment, the isotopic composition of nuclei from Li to Ge was measured [75, 159, 163–167]. These measurements yielded several remarkable results.

ACE-CRIS successfully measured the ^{22}Ne/^{20}Ne isotope ratio with good accuracy: $0.387 \pm 0.007(\text{stat.}) \pm 0.022(\text{syst.})$ [164]. This value implies that the ^{22}Ne/^{20}Ne ratio is larger than that in the solar wind by a factor of 5.3 ± 0.3, which, in turn, suggests that in approximately 20% of cases supernova explosions occur in an environment enriched with the stellar wind of Wolf–Rayet stars, which implies, in turn, that the site of supernova explosions in a very significant number of cases are young OB associations. These results [164] refined and confirmed previous experiments in which an excess of ^{22}Ne was detected. The ACE-CRIS results regarding the fraction of supernova explosions in the stellar wind of Wolf–Rayet stars are consistent with those obtained from charge composition analysis of superheavy cosmic-ray nuclei (see above). These results were used as the basis for further discussion and development of theoretical models of the evolution of star clusters [168].

In the ACE-CRIS data, 15 nuclei of the ^{60}Fe isotope were detected against a background of 3.55×10^5 iron-56 nuclei [167] (see also the first report [166]). The ^{60}Fe/^{56}Fe ratio in the source was determined to be $(7.5 \pm 2.9) \times 10^{-5}$. The detection of supernova-produced ^{60}Fe in cosmic rays implies that the time required for the acceleration and transfer of nuclei to Earth is not much longer than the half-life of ^{60}Fe of 2.6 million years, and that the distance from the ^{60}Fe source to the Sun cannot significantly exceed one kiloparsec. This study provides a very successful example of the use of radioisotope clocks in cosmic-ray physics.

The heaviest nucleus for which the isotopic composition was measured in the ACE-CRIS experiment is the Ge nucleus ($Z = 32$) [75] (no significant differences from the composition of the solar system were found).[3] No experiment has yet provided the isotopic composition for any of the heavier nuclei, and this area of data completely remains *terra incognita*. It should be noted that the issue of determining the isotopic composition of superheavy nuclei heavier than germanium is very urgent, since already for the pair of charges 34 and 38 (Se and Sr) a double r–s peak is observed in the abundance of elements, the study of which would make an important contribution to the exploration of the mechanism of synthesis of superheavy elements; in the range of superheavy nuclei, there are convenient radioisotope clocks: $^{93}_{40}$Zr ($T_{1/2} = 1.52 \times 10^6$ years), $^{93}_{42}$Mo ($T_{1/2} = 0.06 \times 10^6$ years), etc. [169], which could provide important information about the sources and the propagation of cosmic rays.

Some modern direct experiments, focused primarily on measuring the spectra of cosmic rays at high and ultra-high energies, also provide some information about the isotopic composition of cosmic-ray nuclei. Using the time-of-flight system, ionization losses, and the nonuniversality of the trajectory of nuclei in magnetic fields at not too large values of magnetic rigidity, the PAMELA experiment measured the isotopic composition of nuclei ranging from protons to carbon [170–173]. A special feature of this analysis is that the absolute fluxes of isotopes or the ratios of fluxes of various isotopes are always presented as a function of particle energy or magnetic rigidity ranging from hundreds of MV to 5–6 GV. Rarer isotopes may be either of secondary origin or used as radioisotope clocks (such as ^{10}Be and ^{14}C), so these data provide ample material for comparison with models of the origin and propagation of cosmic rays (see the works cited).

The AMS-02 collaboration [107, 174] successfully measured the ^{3}He/^{4}He flux ratio in the magnetic rigidity range of 2–21 GV. The ^{3}He isotope is predominantly of secondary origin; therefore, the information that follows from the ^{3}He/^{4}He ratio is similar to that from the B/C ratio, the difference being that the nuclear path length of helium nuclei is significantly higher than that of carbon nuclei. Due to this, the ratio for helium isotopes will give information about the length of the escape of nuclei from the Galaxy, depending on the magnetic rigidity, which is more averaged over the entire volume of the Galaxy than for carbon nuclei. For the exponent Δ in the dependence of the escape length on the rigidity, $C(R/4\,\text{GW})^{\Delta}$, the value $\Delta = -0.294 \pm 0.004$ was obtained in [174] for the ratio of helium isotopes, which, within two standard deviations, coincides with the value $\Delta = -0.333 \pm 0.014(\text{stat.}) \pm 0.005(\text{syst.})$ obtained for the B/C ratio in the same AMS-02 experiment [144].

A unique result has recently been obtained from new processing of data from the SOKOL-2 experiment. The SOKOL-2 space spectrometer operated aboard the Soviet satellite Cosmos-1713 in 1985 and 1986. The main data from the spectrometer have long been processed and the results obtained published [175]. However, the development of the Monte Carlo technique for simulating the interaction of charged particles with matter and the emergence of new interaction models made it possible to re-process experimental data and obtain new results pertaining to the ratio of deuterium and proton fluxes [176]. Previously, the maximum energy for which this ratio was obtained did not exceed 20 GeV/nucleon (see references in [176]), but in the new processing of SOKOL-2 data this ratio was obtained for the energy range of 0.5–2 TeV/nucleon. Two circumstances were decisive for obtaining this result. First, the SOKOL-2 spectrometer is based on the use of an ionization calorimeter to measure particles, the depth of which is 5.5 inelastic proton path lengths, i.e., the calorimeter is thick for nuclear interaction, unlike all calorimeters of the modern

[3] Binns W R at al. (CRIS collaboration) reported in *Astrophys. J.* **936** 13 (2022) [215] that separation of isotopes was extended to $Z = 38$ (*Author's note to proof*).

PAMELA, AMS-02, FERMI, NUKLON, CALET, and DAMPE experiments mentioned above. The large thickness of the SOKOL-2 calorimeter makes it possible, in principle, to distinguish the longitudinal shape of the developing cascade of deuterons and protons at the same energy per particle, which is directly measured by the calorimeter. However, to distinguish between protons and deuterons based on the cascade shape, a reliable simulation of the cascade curves by Monte Carlo codes is required, i.e., the results are model dependent. The second factor that made it possible to carry out this study was the appearance of a large number of reliably tested Monte Carlo programs with various generators of proton–nucleus and nucleus–nucleus interactions, so systematic errors can be estimated using various codes and generators. In [176], three different methods were compared to show that the systematic errors associated with the model dependence are relatively small. The result of this study was quite unexpected. The fraction of deuterium in the total flux of deuterium and protons is about 10%, which is significantly greater than the value measured at any energies less than 20 GeV/nucleon (no more than 0.03 [176]). Actually, a situation occurs that resembles a sharp kink in the sub-iron-to-iron ratio (see Fig. 15): first, an expected drop is observed in the D/H ratio with increasing energy, but the point obtained in [176], which corresponds to a range of 0.5–2 TeV/nucleon, suggests that in this ratio a sharp upward kink should be exhibited in the curve somewhere between 20 GeV/nucleon and 500 GeV/nucleon. Given that cosmic-ray deuterium is predominantly secondary, the question arises as to whether there is a general mechanism leading to a sharp flattening of the ratio of secondary to primary nuclei at energies from a hundred to several hundred GeV/nucleon.

8. Electrons, positrons, and antimatter

8.1 Total spectrum of electrons and positrons

The lepton component of cosmic rays is represented by a mixture of electrons and positrons, and the simplest task is to measure their total flux, since, in this case, separation of particles by charge is not required. For this task, an ionization calorimeter is an adequate tool, although, of course, the total spectrum can also be measured by magnetic spectrometers, provided the sign of the electric charge is not taken into account. In this subsection, the energy spectrum of electrons is understood as the total spectrum of electrons and positrons. Since, unlike heavy nuclei, light electrons intensively lose energy due to synchrotron radiation in interstellar magnetic fields and inverse Compton scattering from the microwave background and optical and ultraviolet radiation quanta, it is clear that, given the same spectrum in the source, the energy spectrum of electrons should be steeper than that of protons. The difference in spectral indices will be of the order of one half, the exact value depending on the details of the propagation models [13, 177]. In general, it has been clear for a long time that, due to the fact that electrons quickly lose energy, the electron spectrum contains information about the environment of the Sun on a scale of one kiloparsec. Therefore, we can expect the presence in the spectrum of some features associated with nearby sources: averaging of the electron spectrum over the Galaxy does not occur, unlike the spectrum of protons and not too heavy nuclei. This issue has been discussed in a practical sense for a long time in connection with the results of the balloon experiment of Nishimura et al. [178]. For this

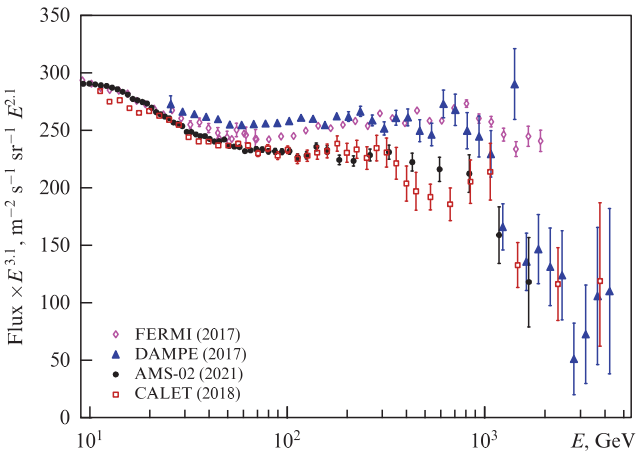

Figure 18. Spectrum of electrons plus positrons according to Fermi [179], DAMPE [180], AMS-02 [107], and CALET [181] direct space experiments.

reason, the two main questions of interest in measuring the energy spectrum of cosmic-ray electrons are how steep the electron spectrum really is and what additional structures can be found in the spectrum besides simple power-law behavior. Both issues currently seem quite confusing.

Figure 18 shows the results of recent (published no earlier than 2017) measurements of the electron energy spectrum in the Fermi [179], DAMPE [180], AMS-02 [107], and CALET [181] experiments. It is worth noting that the AMS-02 experiment first published the electron spectrum in [182]; however, for review [107], the spectrum was reprocessed (intensity values changed slightly), and two new energy points were added, so the limiting energy increased from 837 GeV to 1665 GeV. It should be noted, first of all, that the energy spectra of electrons obtained in direct measurements are very different in nature from the spectra of nuclei in the same experiments. All ionization calorimeters of modern direct experiments are thin to nuclear interactions, due to which the energy resolution of nuclear spectra is very poor, and the spectra require solving the inverse problem (deconvolution) to reconstruct their original form. However, the same calorimeters are thick for electromagnetic interactions, so the energy resolution in electron spectra is much better, and they are well suited for identifying fine structures in them on energy scales of tens of percent or even smaller. Energy resolution in the experiments presented in Fig. 18 varies from 20–30% at energies of the 1 TeV scale in the Fermi and AMS-02 experiments to 2–3% in the CALET and DAMPE experiments. Statistical confidence of measurements of the electron spectrum in the Fermi, AMS-02, CALET, and DAME experiments (Fig. 18) is significantly higher than that in similar measurements in the previous generation of the ATIC [13, 183, 184] and PAMELA [185] experiments, although these older experiments have not lost their significance: they confirm the general behavior of the electron spectra, and the ATIC experiment left behind a mystery that has not yet been solved (see below).

The main feature of all spectra presented in Fig. 18 is their essentially nonpower-law behavior. All experiments consistently indicate a spectral deflection in the region from several tens to about hundreds of GeV, followed by a sharp dip (kink) near 1 TeV (this dip in the Fermi data is somewhat less pronounced than in other experiments, but is also present). It can be argued that the region of the spectrum between

100 GeV and 1 TeV has the shape of a wide bump against the background of a power-law spectrum with a spectral index somewhat greater than three. The existence of such a bump was first reported in the ATIC experiment [183], although its shape there is even more pronounced than in the curves displayed in Fig. 18. The existence of a kink near 1 TeV was confirmed by the ground-based Cherenkov telescopes H.E.S.S. [186], MAGIC [187], and VERITAS [188].

The exact reason for the emergence of the global feature of the electron spectrum in the form of a 100–1000 GeV bump is currently unclear. It is usually associated with one or more nearby discrete sources (often, theoretical papers only consider the kink near 1000 GeV). By now, several hundred articles have been published addressing this set of issues; however, analyzing them is beyond the scope of this review. Several different hypotheses of this type, together with references to some previous work, can be found in recent paper [189].

Although experiments, the data of which are displayed in Fig. 18, suggest a qualitatively similar picture, the difference in the details of this behavior is large and goes beyond the statistical and expected systematic errors. The experiments are divided into two groups, one of which includes Fermi and DAMPE, and the other, AMS-02 and CALET. Each of these groups yields within itself a similar behavior of the spectra in the energy range of 100–1000 GeV, but these two groups differ significantly from each other. The reasons for this difference are not yet clear: they may be systematic errors unaccounted for, but external physical mechanisms cannot be ruled out. In particular, it may be noted that the experiments are carried out at different heights. The AMS-02 and CALET instruments are installed aboard the International Space Station and take measurements under identical conditions at an average orbital altitude of about 420 km, while the orbital altitudes of the Fermi and DAMPE observatories are about 530 and 500 km, respectively.

In addition to the general behavior of the electron spectrum, as already noted, of interest is the presence of small features in the form of narrow peaks, bumps, or dips that could be associated with local sources. In a range from 100 to 1000 GeV, the spectra in Fig. 18 do not exhibit a statistically significant structure, and no correlation is observed in the small-scale behavior of these spectra (on the scale $\Delta E \sim 100$ GeV). In the CALET data, a depression can be seen in the range from about 400 to 700 GeV, but it is not statistically significant. In the energy range above 1000 GeV, at the spectral point with an energy of 1411.4 GeV, there is a sharp outlier in the DAMPE data, which is not confirmed by any other experiment. In the original DAMPE paper [180], this outlier is not specifically discussed in any way, and, apparently, it may be understood as a statistical fluctuation.

The Fermi, DAMPE, AMS-02, and CALET experiments failed to solve the mystery that the ATIC experiment left behind. In the ATIC stratospheric experiment, the spectrometer, the design of which is very similar to that of the DAMPE and CALET calorimetric spectrometers, made three flights around the South Pole, of which two flights, ATIC-2 (December 29, 2002 to January 18, 2003) and ATIC- 4 (December 26, 2007 and January 15, 2008) were successful and yielded many new results. Among other things, the spectrum of electrons was measured on each of these flights. The electron spectra measured on both ATIC-2 and ATIC-4 flights were published in [184, 190] and, in the given spectra, rather fine energy binning was used with an equidistant step

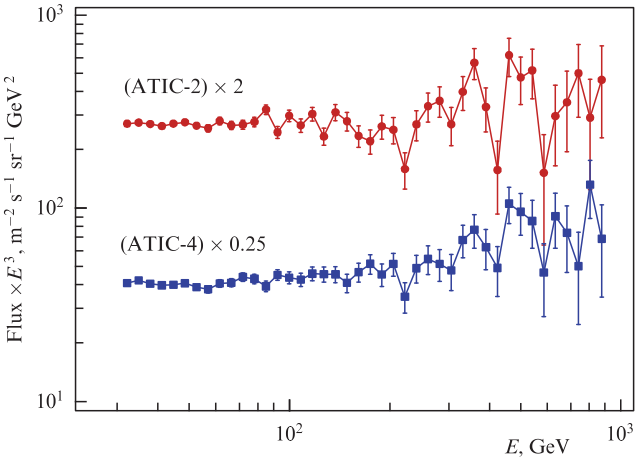

Figure 19. Fine structure of electron spectra according to data from ATIC experiment (flights of ATIC-2 and AT1S-4 spectrometers presented separately) [184, 190].

of 0.035 in the logarithm of energy ($\Delta E/E = 8.4\%$). In a range between 200 and 700 GeV, the measured spectra revealed a fine structure of the spectrum of very large amplitude, represented by peaks near 250, 350, and 500 GeV, and this structure was well reproduced in both flights of the ATIC-2 and ATIC-4 spectrometer (Fig. 19). It should be stressed that the ATIC-2 and ATIC-4 spectrometers were not identical instruments. In particular, they contained calorimeters of different depths (18 and 22 cascade units, respectively [184, 190]). This implies that the discovered fine structure cannot be a consequence of the design features of the spectrometer, since the spectrometers were different.

Two different methods were used to determine the statistical significance of fine structure. First, the statistical significance of the correlation (similarity) of the structure of the spectra measured separately in the ATIC-2 and ATIC-4 flights was determined; second, the statistical significance of the presence of a nonrandom structure was determined using the usual criterion χ^2 for the total ATIC-2 + ATIC-4 spectrum. In both cases, statistical significance was close to three standard deviations [184, 190]. This implies that the observation is not yet a discovery, but a strong indication of the existence of an effect.

To rule out methodological reasons for the emergence of the discovered structure, a number of tests were carried out [184, 190]. Various methods have been explored to filter electron events from the proton background; electron spectra were studied for various solid angles and various durations of the experiment, etc. The fine structure was reproduced in all cases. Various energy binning of spectra were examined. It is shown that the fine structure is not a binning artifact, but is well manifested at any binning starting from 0.035 in the energy logarithm and finer. Thus, there was no indication that the fine structure detected could be a result of methodological effects. With energy binning coarser than 8.4% (0.035 in logarithm), the fine structure quickly ‘sinks’ into energy bins that are too wide (as, for example, in the first publication of the ATIC-1 electron spectrum [183]), so one should not expect that a fine structure similar to that revealed in the ATIC-2 and ATIC-4 experiments [184, 190] will be visible in the modern experiments shown in Fig. 18, since none of these experiments used binning finer than 15% (0.06 in logarithm).

To check the ATIC result, it is necessary not only to use adequate, fairly fine energy binning but, strictly speaking, also to measure the electron spectrum in the southern circumpolar region of Earth, where the ATIC experiment was carried out, since at present it is not possible to exclude the anisotropy of the electronic spectrum: electron spectra measured for different directions of incoming electrons with energies of hundreds of GeV, in principle, may turn out to be different. None of these requirements have yet been fulfilled, so the enigma of the fine structure of the electron spectrum of the ATIC experiment persists. It should be noted that verifying these results is also very urgent, since a fine structure similar to that discovered in the ATIC experiment may be a signature of the contribution of pulsars, rather than dark matter, to such features of the spectra of electrons and positrons as excess in the positron flux discovered in the PAMELA experiment [12]. In theoretical paper [12], it was shown that the fine structure of the electron spectrum, very similar to that found by the ATIC experiment, can be due to contributions from several nearby pulsars (this paper was published before the discovery of the fine structure, i.e., this assertion can be considered its prediction), and it was shown in [13] that, with reasonable assumptions about the initial energy range and spectra of electrons and positrons accelerated in pulsar nebulae, several nearby pulsars could provide the specifically discovered fine structure of the electron spectrum.

8.2 Antimatter in cosmic rays

Until 2009, it was generally believed that antiparticles in cosmic rays were predominantly of secondary origin, resulting from the interaction of primordial cosmic rays, which consist of ordinary matter, with interstellar gas [177]. The situation changed dramatically after the publication of the result of the PAMELA experiment [191]. It was found that, at energies above about 5 GeV, instead of the drop expected in the proportion of positrons in the total flux of positrons and electrons with increasing energy if the positrons are of secondary origin, a sharp increase is observed in the ratio up to energies on the scale of 100 GeV, above which the PAMELA experiment could not advance due to a lack of statistics. It became clear that it was necessary to look for sources of positrons other than the interaction of primordial cosmic rays with the interstellar medium, and dozens of theoretical papers were immediately published discussing the primary sources of antimatter in cosmic rays, such as annihilation or decay of dark matter, pulsars, etc., although attempts to reconcile the result obtained with the purely secondary origin of antiparticles in cosmic rays continued for some time. An analysis of some early studies discussing the positron anomaly and related issues can be found in review [13].

Already in the first PAMELA paper [191], the annihilation or decay of dark matter particles was discussed as the main circumstance explaining the positron anomaly, but the creation and acceleration of positrons in such nearby sources as the magnetospheres of pulsars and microquasars were also mentioned. Any of the mechanisms should feature a certain limit on the energy of positrons, characteristic of a given source; therefore, to establish the nature of the phenomenon, it was necessary, first of all, to reveal this limit in the experimental data. In addition, confirmation of the phenomenon in independent experiments was required. The first confirmation of the positron anomaly was obtained by the Fermi space observatory [192] (2011), and the energy reached

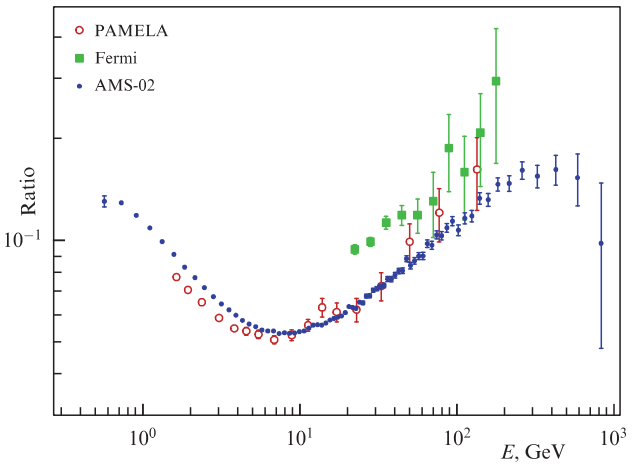

Figure 20. Ratio $e^+/(e^+ + e^-)$ according to PAMELA [195], Fermi [192], and AMS-02 [107, 182] experiments.

200 GeV. No signs of the end of the growth of the ratio $e^+/(e^+ + e^-)$ with increasing energy were found. Starting in 2013, the AMS-02 collaboration started producing results, and, as statistics accumulated, published the ratio $e^+/(e^+ + e^-)$ three times with a gradually increasing upper limit of the measured energy [107, 182, 193, 194]. In the second of the articles, the energy was increased to 420 GeV, and it was already noted that at energies above 200 GeV there was no increase in the ratio; however, in publications [107, 182], the limiting energy was already 830 GeV, and a fairly pronounced drop in the ratio was observed. Figure 20 shows recent results for the positron-electron ratio from the PAMELA [195], Fermi [192], and AMS-02 [107, 182], experiments. It should be stressed that the PAMELA results [195] have been updated compared to the first publication [191] (in particular, the limiting energy has been increased to 135 GeV). For a better understanding of the data displayed in Fig. 20, it should be noted that the PAMELA and AMS-02 magnetic spectrometers can distinguish positrons from electrons by the sign of the trajectory curvature in a magnetic field, but the Fermi observatory, operating based on an ionization calorimeter, itself does not distinguish electrons from positrons. To separate the fluxes of electrons and positrons, the authors of [192] used the anisotropy of the flow of charged particles in Earth's magnetic field. The systematic uncertainties of this technique are much larger than those of the direct technique of the PAMELA and AMS-02 experiments, so it is not surprising that the difference between Fermi data and those of PAMELA and AMS-02 exceeds statistical errors. The PAMELA and AMS-02 results are statistically consistent for energies above 10 GeV, and small differences at energies below 10 GeV may be due to differences in solar modulation.

According to [107, 182], the excess of positrons can be ascribed to an additional source, which has a distribution with a maximum of 284^{+64}_{-91} GeV for the spectrum of the source multiplied by E^3. This observation can be used to make some conclusions about the source of the positrons, but it is still insufficient to distinguish between dark matter annihilation and pulsars. A critical signature for making such a distinction may be the detection of additional fine structure, which can be found in both electron and positron spectra and in the $e^+/(e^+ + e^-)$ ratio [12, 13]. The energy scale at which such fine structure can be observed may not be

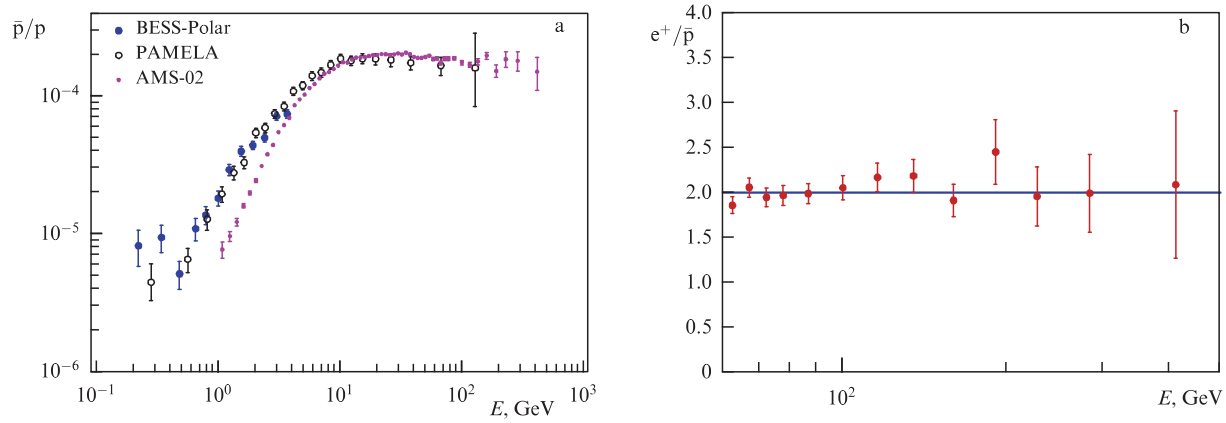

Figure 21. (a) Ratio $\bar{p}/p$ from BESS-Polar [197], PAMELA [198], and AMS-02 [107] experiments. (b) Ratio $e^+/\bar{p}$ based on data from AMS-02 [107].

less than 100 GeV; it is expected at energies above 200 GeV, and a modulation amplitude in the ratio $e^+/(e^+ + e^-)$ that would correspond to the fine structure found in the ATIC experiment ([184, 190]; see above) should be on the order of 30% [13]. The occurrence of such a fine structure suggests that the source of the positron anomaly is several nearby pulsar nebulae and excludes the decay or annihilation of dark matter. The detection of such a fine structure in the $e^+/(e^+ + e^-)$ ratio is beyond the capabilities of the AMS-02 experiment due to both insufficient energy resolution and lack of statistics. To identify the desired fine structure, a new generation of experiments is needed that would be able to simultaneously provide an energy resolution in the spectrum of electrons and positrons of no worse than 5% (which is easily achieved using sufficiently thick ionization calorimeters) and statistics numbering significantly more than those of the AMS-02 experiment.

Some light on the nature of the positron anomaly could be shed by data on the flux of antiprotons in cosmic rays, since those positrons and cosmic-ray antiprotons that are not of purely secondary origin may have common sources. The antiproton spectrum was measured in the BESS-TeV [196], BESS-Polar [197], PAMELA [198], and AMS-02 [107, 199] experiments and in many earlier experiments. Figure 21a presents the results of the BESS-Polar [197], PAMELA [198], and AMS-02 [107] experiments for the antiproton to proton flux ratio. A notable feature of the $\bar{p}/p$ ratio is the very slow decrease in the curve at energies above 20 GeV. If antiprotons had a secondary origin, primarily as products of the scattering of cosmic ray protons on interstellar gas, the $\bar{p}/p$ ratio should fall with an energy similar to the B/C ratio (see Fig. 12). However, this does not occur, implying that there is some additional source of antiprotons. In this respect, the situation with antiprotons is quite similar to the PAMELA positron anomaly. Figure 21b shows the ratio of the spectrum of positrons to antiprotons according to the latest AMS-02 data [107]. The ratio for energies above 60 GeV turns out to be close to the constant which was determined in [107] as $2.00 \pm 0.03(\text{stat.}) \pm 0.06(\text{syst.})$. Should antiprotons and positrons originate from the same source, and, in this source, they had the same initial spectra of magnetic rigidity, as should have been the case during acceleration on a shock wave of a supernova remnant or a shock wave of a different origin, the measured spectrum of positrons would turn out to be steeper than that of antiprotons, since positrons, with increasing energy, unlike antiprotons, begin to quickly lose energy due to inverse Compton scattering and synchrotron radiation. Therefore, the measured constant ratio rather indicates that the initial spectra of antiprotons and positrons are different (the spectrum of positrons should be harder). For a better understanding, it is necessary to see in the experimental data the limit of the acceleration of antiprotons, which would better clarify the nature of the source, but for this, not a single experiment provides sufficient statistics. Thus, although the questions about the origin of the excess of positrons and the excess of antiprotons turn out to be related, neither of them has been answered.

Heavier antinuclei are also searched for in cosmic rays. The PAMELA collaboration sets an upper limit on the $\overline{\text{He}}/\text{He}$ flux ratio [200]: for a magnetic rigidity of nuclei above 14 GV, $\overline{\text{He}}/\text{He} < 4.7 \times 10^{-7}$. Some references to oral sources (reports at conferences) mention that eight candidates for antihelium nuclei were detected in the AMS-02 experiment [201, 202]. However, the AMS-02 collaboration has not published these data, so methodological details regarding this information are not yet available. In any case, it is clear that the flux of antihelium nuclei (and, of course, heavier antinuclei) is very small, so further progress in this field requires instruments with both a very large geometric factor and the ability to distinguish the sign of particle charges.

9. Prospects and future experiments

The most urgent tasks of cosmic ray physics are currently the determination of the chemical composition of abundant CRs with the maximum possible advancement up the energy scale and the identification of the charge (isotopic) composition of superheavy CR nuclei behind the iron peak. Both of these CR components were produced in the most catastrophic processes in the Galaxy, and it is based on them that modern models are built. CRs also provide an option for dedicated searches for exotic phenomena that could yield experimental evidence of the existence of dark matter particles or detect strange matter particles.

As before, these studies are focused on an astrophysical interpretation of the Christiansen–Kulikov 'knee' phenomenon in the energy region of $\sim 3 \times 10^{15}$ eV. The key to solving this problem may be a statistically reliable determination of the chemical composition of CRs in this energy range.

As shown above, in recent years, studies of CRs in the energy range of tens and hundreds of TeV have revealed a

number of features in the chemical composition and energy spectra that have deep astrophysical implications. With an increase in the number of statistics and accuracy in energy measurements, both new discoveries and confirmation of already obtained indications can be predicted.

Knowledge about the Galaxy will be incomplete without studying the second most important component of CRs: the charge (isotopic) composition of superheavy CR nuclei behind the iron peak. These data contain information about galactic nucleosynthesis in the modern cosmological era and determine the parameters of outer space in the near region of the Galaxy.

The search for antimatter is also of great interest. At present, only the spectrum of antiprotons has been studied.

Exploring the spectra of electrons and positrons is of utmost importance in what regards studying nearby sources and searching for dark matter.

The solution to these problems is of importance both per se and for the development of new astrophysical models in combination with astronomical observation data in various ranges. A comparison of data obtained for various CR components (hadrons, electrons, positrons, gamma quanta) in various energy ranges constitutes a fairly new approach — multi-messenger astronomy. Now, a search for new signatures for dark matter is needed that would take into account the constraints on the properties of weakly interacting massive particles established by experiments at the LHC. Various hypotheses about the nature of dark matter are considered, most of which go beyond the Standard Model.

The variety of basic problems being examined sets the study of CRs as a priority task in cosmic physics. Despite the extremely high cost of such studies due to a fairly limited set of research technologies and the need to move massive equipment outside the atmosphere, several significant experiments are scheduled for the near future.

9.1 TIGERISS experiment

The TIGERISS (Trans-Iron Galactic Element Recorder for the ISS) experiment [203, 204] will measure nuclear fluxes from boron to lead at energies above 350 MeV/nucleon. This is a further development of the TIGER and SuperTIGER balloon experiments with improved charge resolution and extended dynamic energy range from 350 MeV/nucleon to 10 GeV/nucleon. Long-term exposure is expected when placing scientific equipment on the International Space Station.

The equipment consists of two crossed layers of silicon detectors located at the top and bottom of the device, which determine the trajectories of particles and the amount of ionization ($\mathrm{d}E/\mathrm{d}x$). The nuclear charge Z and energy E are measured by two Cherenkov detectors containing an acrylic emitter (optical refractive index $n = 1.49$) and a quartz air-gel emitter ($n = 1.04$). The estimated maximum possible geometric factor of the equipment is 1.66 m^2 sr [204]. Figure 22 shows the statistics expected for 5 years of exposure at an average value of solar modulation.

9.2 NUKLON-2 experiment

The NUKLON-2 space experiment [169] is designed to study the charge and isotopic composition of superheavy cosmic ray nuclei in the charge range $Z = 6-92$ at energies above 100 MeV. The NUKLON-2 recording equipment consists of a set of identical multilayer (40 layers) ionization calorimeters made of silicon detectors (Fig. 23a). The parameters of the

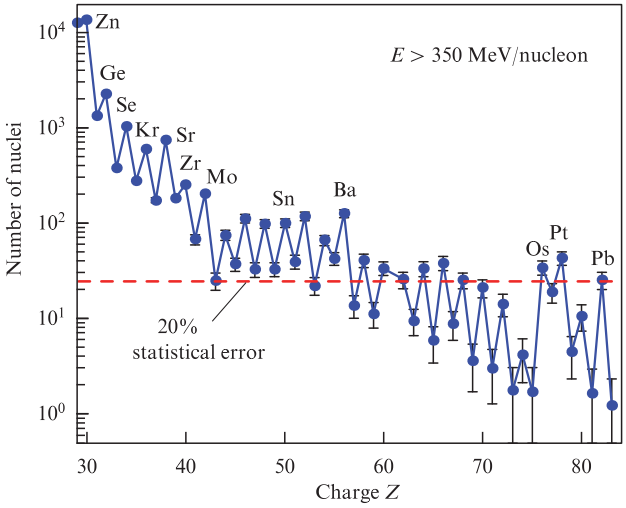

Figure 22. Expected statistics for 5 years of TIGERISS exposure.

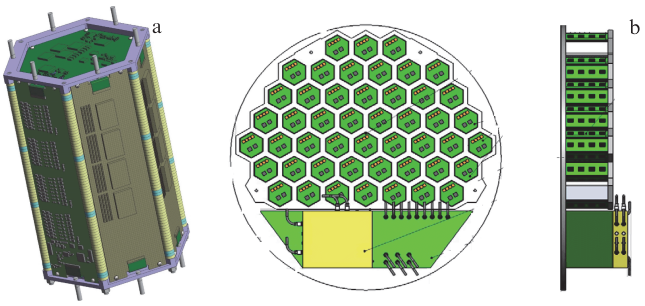

Figure 23. Scientific equipment of NUKLON-2: (a) design view of the unit; (b) example of an assembly of 48 identical modules.

CR projectile nucleus are determined using a well-known method for measuring the MZ^2 product (Z is the charge, M is the mass number). The method is based on the simultaneous measurement of the total energy of the nucleus E deposited in the bulk of the spectrometer and the energy losses $\mathrm{d}E/\mathrm{d}x$ when passing through a thin detector of thickness $\mathrm{d}x$. The product $E \times (\mathrm{d}E/\mathrm{d}x) \propto MZ^2[\ln E + \mathrm{const}]$, which determines Z and M. The proposed method was successfully applied, including in a number of space experiments, to determine the isotopic composition of CRs up to $Z \sim 30$ (see, in particular, [75]). When moving to heavier nuclei, the efficiency of this technique deteriorates, since the useful signal by which isotopes are separated becomes comparable to the level of physical fluctuations. For the NUKLON-2 experiment, the technique was optimized using multiparameter analysis for a multilayer ionization calorimeter, which extended the ability to separate isotopes for elements with charges up to $Z \sim 60$.

Scientific equipment is designed as a frame structure (Fig. 23b). The figure shows an example of an assembly consisting of 48 modules. The mass of the equipment in this case is less than 400 kg, and the geometric factor is $\sim 1.7\,\mathrm{m}^2$ sr. Due to the modular design, the number of spectrometers can be increased or decreased in accordance with the size and mass restrictions of the space platform.

NUKLON-2 is the most significant current project in this area of research, where information is quite limited. For example, above the region $Z = 32$, information on the isotopic composition of cosmic rays is a 'blank spot';

Table 1. Expected statistics from NUKLON-2 experiment for a 5-year exposure.

Nucleus, Z	N	Nucleus, Z	N
Fe 26	3×10^7	Zr 40	500
Co 27	1.4×10^5	Nb 41	150
Ni 28	1.1×10^6	Mo 42	230
Cu 29	1.6×10^4	Ru 44	100
Zn 30	1.6×10^4	Ag 47	140
Ga 31	2000	Cd 48	120
Ge 32	2300	Sn 50	120
As 33	350	Te 52	140
Se 34	1400	Xe 54	80
Br 35	200	Ba 56	180
Kr 36	830	Ce 58	50
Rb 37	250	Nd 60	40
Sr 38	1000	Dy 66	180
Y 39	250		

NUKLON-2 exceeds the exposure factor of the ACE CRIS experiment by a factor of 20 and will extend studies of the isotopic composition to $Z \sim 60$. NUKLON-2 will increase the number of available statistics of the SuperTIGER experiment by approximately an order of magnitude. Table 1 shows the expected statistics on the isotopic composition of the NUKLON-2 experiment for 5 years of exposure.

9.3 HERD experiment

The launch of the HERD (High Energy cosmic-Radiation Detection facility) [205] equipment to the Chinese orbital station is scheduled for 2027. This is a large-scale, multi-purpose, high-energy astrophysical experiment. It is planned to measure the fluxes of electrons and gamma rays from 100 MeV to tens of TeV and nuclei CRs with $Z = 1-26$ in the energy range from 30 GeV to several PeV. The experiment will feature a fairly high energy resolution: for the leptonic component, of a unit of percent, and, for the nuclear component, at a level of 20%.

The HERD equipment includes a small-section 3D calorimeter (7500 cubes of LYSO scintillator, edge length 3 cm); the calorimeter being surrounded with a scintillation tracker, a plastic scintillation detector, and a silicon charge detector matrix.

The geometric factor of the device is estimated to be ~ 2 m^2 sr for protons and ~ 3 m^2 sr for electrons. It is planned to measure the total spectrum of electrons and positrons up to tens of TeV over five years and test the hypothesis about the presence of a deflection associated with the properties of dark matter. The spectrum of protons will be measured up to several PeV; the spectra of individual nuclei, up to several hundred TeV/nucleon, and thus detailed information will be obtained about the properties of cosmic rays in the 'knee' region. It is also planned to measure gamma-ray fluxes up to 100 TeV in a very wide aperture, including searching for accompanying gravitational waves and neutrino events. Peaks in the gamma spectrum associated with the possible annihilation of dark matter particles will also be searched for.

9.4 HERO experiment

The main purpose of the HERO (High Energy Ray Observatory) experiment [206, 207] is to provide, along with precision measurements of the parameters of CR spectra, the maximum possible exposure factor, with the aim of extending the energy scale of the cosmic ray spectrum. The objectives of the experiment include the measurement of fluxes of CR nuclei in the entire charge range $Z = 1-92$ with element-wise resolution in an energy range from 10^{12} to 10^{16} eV/particle and fluxes of electrons and gamma rays from 300 GeV to tens of TeV. A large exposure factor is achieved due to the significant dimensions and weight of the scientific equipment: the minimum permissible weight of HERO is 16 tons. With this mass of the equipment, the effective geometric factor is, for protons, ~ 12 m^2 sr, for nuclei, ~ 16 m^2 sr, and for electrons and gamma quanta, ~ 20 m^2 sr. The energy measurement accuracy is, for protons in the region from 10^{15} to 10^{16} eV, 30%, and for protons below 10^{15}eV and nuclei, 10–20% (depending on the type of nucleus and energy). The accuracy of energy measurements for electrons and gamma quanta is ~ 1%. All technologies used to produce HERO were successfully tested in the NUKLON space experiment (see Section 2). One of the main prerequisites of the HERO astrophysics experiment is the use of a heavy or super-heavy class launch vehicle.

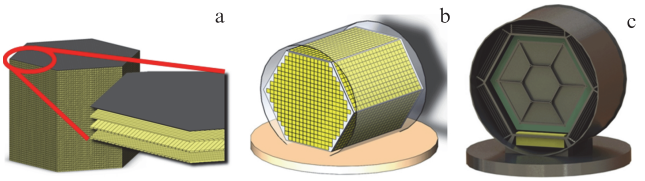

Figure 24. Design view of the HERO equipment: (a) design view of the ionization calorimeter, (b) design view of the energy measurement system, (c) general view of the assembled HERO.

The HERO orbiting observatory consists of two main recording systems: an ionization calorimeter and a system for measuring (or recording the absence of) the charge of an incident particle. The IC contains 62 hexagonal detectors, each of which consists of a ~ 2 mm tungsten sheet and three layers of scintillation strips, each 8 mm high. Light is collected through optical fibers laid in the grooves of the strips; the strips themselves are placed in three directions at angles of 0°, 60°, 120° (Fig. 24a). A charge measurement system located around the calorimeter (Fig. 24b) is a four-layer silicon pad matrix, with a pad size of 1 cm^2. Due to the finely granular structure of the matrix, the charge measurement technique is resistant to reverse current and provides a resolution of no worse than 0.2 charge units in the region of CNO peaks. Structurally, the HERO equipment is placed in a thermal container (Fig. 24c) mounted on the platform of the base spacecraft with the maximum possible visibility.

The main goals of the HERO experiment are to determine the chemical composition of CRs with element-wise charge resolution in the Christiansen–Kulikov knee region (energy $\sim 3 \times 10^{15}$ eV); to study abundant CRs in the region behind the 'knee', up to 10^{16} eV; to precisely determine the composition of CRs in the energy range of $10^{12} - 10^{15}$ eV (high number of statistics and energy resolution), including for rare secondary nuclei; to study the anisotropy of CRs with the number of statistics exceeding existing ones by more than two orders of magnitude; to study the electronic spectrum in the energy range up to tens of TeV; to examine nuclei beyond the iron peak, including superheavy exotic nuclei; to measure the diffuse spectrum of gamma radiation

Table 2. Comparative characteristics of the most successful implemented and some scheduled experiments.

Name	Years	Geometric factors, m^2 sr year	Energy range, eV/nucleon (particle)	Components under study
CRIS	From 1997	0.38	$10^7 - 10^8$	Nuclei
PAMELA	From 2006	0.02	$< 2 \times 10^{11}$	Nuclei Electrons
AMS02	From 2011	5	$< 2 \times 10^{12}$	Nuclei Protons
CREAM	Before 2012	0.5	$10^{11} - 10^{14}$	Nuclei Electrons
Fermi	From 2008	10	$2 \times 10^7 - 3 \times 10^{12}$	Gamma particles Electrons
CALET	From 2015	0.5	$10^9 - 2 \times 10^{13}$	Nuclei Electrons Gamma particles
NUKLON	2015	2.4	$10^{11} - 5 \times 10^{14}$	Nuclei
DAMPE	From 2015	1	$10^{11} - 10^{15}$	Nuclei Electrons Gamma particles
ISS-CREAM	From 2017	~ 5	$10^{12} - 10^{15}$	Nuclei Electrons
TIGERISS	?	~ 1.6	$3 \times 10^8 - 10^{10}$	Nuclei
HERD	From 2027	10	$10^{11} - 10^{15}$	Nuclei Electrons Gamma particles
HERO	After 2030	> 140	$10^{11} - 5 \times 10^{16}$	Nuclei Electrons Gamma particles

over a wide energy range with high energy resolution; to search for products of the interaction of dark matter; and to search for strongly interacting 'strange' matter or to search for the upper threshold of its abundance in the Galaxy.

By its characteristics, HERO is a 'breakthrough' experiment that will set the directions of research in the astrophysics of high-energy particles for the coming decades. A set of statistics is expected at a level of 5 billion events with individual particle charge resolution at a lower detection threshold of about 1 TeV per particle. The specified number of data will exceed by more than two orders of magnitude the global data bank collected over almost 60 years of research in this field of natural science, with qualitatively improved characteristics.

The HERO project has passed all R&D stages and is included in the Federal Space Program of Russia. The implementation of the experiment is scheduled for 2026 through 2035. The project is being developed taking into account the commissioning of new domestic heavy (Soyuz 5V[4]) and super-heavy (Angara 5V[5]) class launch vehicles. If these launch vehicles are manufactured on an industrial scale, given a high level of technological readiness and a relatively low cost of scientific equipment, the implementation of a space experiment is quite realistic.

Table 2 shows comparative characteristics of the most successful and significant planned experiments.

[4] https://www.roskosmos.ru/28990/
[5] https://www.roskosmos.ru/36320/

10. Conclusions

It may be asserted that over approximately the last 15 to 20 years, the appearance of CR physics has changed drastically. From very simplified models such as the universal power-law behavior of spectra, due to the development of techniques for direct observations of CRs, CR physics advanced to studying the subtle features of the behavior of energy spectra, which are considered to be signatures of complex and diverse phenomena in space. Enigmas still persist, especially the almost complete lack of information about the chemical composition of CRs in the region of the Kulikov–Christiansen knee and the associated inability to definitively understand the nature of the knee. It is also worth mentioning the complete lack of information about the isotopic composition of CRs in the region of superheavy nuclei. However, the next generation of instruments for direct observation of CRs in outer space gives us hope that these problems will be solved.

11. Appendix

A. Abbreviations

CRs — cosmic rays
GCRs — galactic cosmic rays
EAS — extensive atmospheric shower
BGO — bismuth germanate oxide $Bi_4Ge_3O_{12}$
IC — Ionization Calorimeter
KLEM — Kinematic Lightweight Energy Meter
ISM — InterStellar Medium
MSM — Massive Star Material
TRD — Transition Radiation Detector

B. Abbreviated names of experiments and projects

ACE — Advanced Composition Explorer
AMS — Alpha Magnetc Spectrometer
ATIC — Advanced Thin Ionization Calorimeter
CALET — CALorimetric Electron Telescope
CREAM — Cosmic-Ray Energetics And Mass
CRIS — Cosmic-Ray Isotope Spectrometer
DAMPLE — DArk Matter Particle Experiment
GRAPES — Gamma Ray Astronomy PeV Energies
HEAO — High Energy Astronomy Observatory
HERD — High Energy cosmic-Radiation Detection facility
HERO — High Energy Ray Observatory
H.E.S.S. — High Energy Stereoscopic System
HNE — Heavy Nuclei Experiment
ISS — International Space Station
LDEF — Long Duration Exposure Facility
MAGIC — Major Atmospheric Gamma Imaging Cherenkov
PAMELA — Payload for Antimatter Matter Exploration and Light-nuclei Astrophysics
TIGER — Trans-Iron Galactic Element Recorder
TRACER — Transition Radiation Array for Cosmic Energetic Radiation
VERITAS — Very Energetic Radiation Imaging Telescope Array System

References

1. Witten E *Phys. Rev. D* **30** 272 (1984)
2. Shaulov S B et al. *JETP Lett.* **116** 1 (2022); *Pis'ma Zh. Eksp. Teor. Fiz.* **116** 3 (2022)
3. Ptuskin V S *Phys. Usp.* **53** 958 (2010); *Usp. Fiz. Nauk* **180** 1000 (2010)
4. Porter T A, Strong A W, astro-ph/0507119
5. Beck R *Proc. Int. Astron. Union* **4** (S259) 3 (2008) https://doi.org/10.1017/S1743921309030014; arXiv:0812.4925
6. Ginzburg V L, Syrovatskii S I *The Origin of Cosmic Rays* (Oxford: Pergamon Press, 1964); Translated from Russian: *Proiskhozhdenie Kosmicheskikh Luchei* (Moscow: Izd. AN SSSR, 1963)
7. Murzin V S *Vvedenie v Fiziku Kosmicheskikh Luchei* (Introduction into Physics of Cosmic Rays) (Moscow: Atomizdat, 1979)
8. Berezhko E G *JETP Lett.* **33** 399 (1981); *Pis'ma Zh. Eksp. Teor. Fiz.* **33** 416 (1981)
9. Zirakashvili V N, Ptuskin V S, Rogovaya S I *Mon. Not. R. Astron. Soc.* **519** L5 (2023)
10. Stozhkov Yu I *Bull. Russ. Acad. Sci. Phys.* **75** 323 (2011); *Izv. Ross. Akad. Nauk Ser. Fiz.* **75** 352 (2011)
11. Panasyuk M I, Miroshnichenko L I *Phys. Usp.* **65** 379 (2022); *Usp. Fiz. Nauk* **192** 413 (2022)
12. Malyshev D, Cholis I, Gelfand J *Phys. Rev. D* **80** 063005 (2009)
13. Panov A D *J. Phys. Conf. Ser.* **409** 012004 (2013)
14. Krymskii G F *Sov. Phys. Dokl.* **22** 327 (1977); *Dokl. Akad. Nauk SSSR* **234** 1306 (1977)
15. Bell A R *Mon. Not. R. Astron. Soc.* **182** 147 (1978)
16. Bell A R *Mon. Not. R. Astron. Soc.* **182** 443 (1978)
17. Axford W I, in *Intern. Cosmic Ray Conf., 17th, Paris, France, July 13–25, 1981, Conf. Papers* (Essonne, France: Gif-sur-Yvette, 1982) p. 155
18. Axford W I, in *Origin of Cosmic Rays. Proc. of the Symp., Bologna, Italy, June 11–14, 1980* (Dordrecht: D. Reidel Publ. Co., 1981) p. 339
19. Jones F C *Astrophys. J. Suppl.* **90** 561 (1994)
20. Vladimirov A E et al. *Astrophys. J.* **752** 68 (2012); arXiv:1108.1023
21. Bell A R, Lucek S G *Mon. Not. R. Astron. Soc.* **321** 433 (2001)
22. Ptuskin V S, Zirakashvili V N *Astron. Astrophys.* **429** 755 (2005)
23. Berezhko E G *Adv. Space Res.* **41** 429 (2008)
24. Hristiansen G B, Kulikov G V *Nuovo Cimento* **8** 742 (1958)
25. Zatsepin V I et al. *Bull. Russ. Acad. Sci. Phys.* **68** 1780 (2004); *Izv. Ross. Akad. Nauk Ser. Fiz.* **68** 1593 (2004)
26. Yoon Y S et al., in *Proc. of the 31st Intern. Cosmic Ray Conf., ICRC 2009, Lodz, Poland, 7–15 July 2009* Vol. 2 (Red Hook, NY: Curran Associates, Inc., 2009) p. 1448
27. Yoon Y S et al. *Astrophys. J.* **728** 122 (2011)
28. Yoon Y S et al. *Astrophys. J.* **839** 5 (2017)
29. Adriani O et al. *Science* **332** 69 (2011)
30. Aguilar M et al. (AMS Collab.) *Phys. Rev. Lett.* **114** 171103 (2015)
31. Aguilar M et al. (AMS Collab.) *Phys. Rev. Lett.* **115** 211101 (2015)
32. Panov A D, Sokolskaya N V, Zatsepin V I *Astrophys. J.* **837** 77 (2017)
33. Panov A D et al. *Bull. Russ. Acad. Sci. Phys.* **71** 494 (2007); *Izv. Ross. Akad. Nauk Ser. Fiz.* **71** 512 (2007); astro-ph/0612377
34. Panov A D et al. *Bull. Russ. Acad. Sci. Phys.* **73** 564 (2009); *Izv. Ross. Akad. Nauk Ser. Fiz.* **73** 602 (2009); arXiv:1101.3246
35. Ahn H S et al. *Astrophys. J. Lett.* **714** L89 (2010); arXiv:1004.1123
36. Prosin V V et al. *Bull. Russ. Acad. Sci. Phys.* **83** 1016 (2019); *Izv. Ross. Akad. Nauk Ser. Fiz.* **83** 1117 (2019)
37. Turundaevskiy A N et al. *Bull. Russ. Acad. Sci. Phys.* **85** 353 (2021); *Izv. Ross. Akad. Nauk Ser. Fiz.* **85** 478 (2021)
38. Atkin E et al. *Nucl. Instrum. Meth. Phys. Res. A* **770** 189 (2015)
39. Grigorov N L, Murzin V S, Rapoport I D *Sov. Phys. JETP* **7** 348 (1958); *Zh. Eksp. Teor. Fiz.* **34** 506 (1958)
40. Fabjan C W, Ludlam T *Annu. Rev. Nucl. Part. Sci.* **32** 335 (1982)
41. Adams J et al. *AIP Conf. Proc.* **504** 175 (2000)
42. Adams J et al. *Adv. Space Res.* **27** 829 (2001)
43. Korotkova N A et al. *Phys. Atom. Nucl.* **65** 852 (2002); *Yad. Fiz.* **65** 884 (2002)
44. Bashindzhagyan G L et al. *Instrum. Exp. Tech.* **48** 32 (2005); *Prib. Tekh. Eksp.* (1) 46 (2005)
45. Podorozhnyi D M et al. *Phys. Atom. Nucl.* **68** 50 (2005); *Yad. Fiz.* **68** 51 (2005)
46. Guzik T G et al. *Adv. Space Res.* **33** 1763 (2004)
47. Panov A D et al. *Instrum. Exp. Tech.* **51** 665 (2008); *Prib. Tekh. Eksp.* (5) 33 (2008)
48. Ahn H S et al. *Nucl. Instrum. Meth. Phys. Res. A* **579** 1034 (2007)
49. Ahn H S et al. *Nuc. Phys. B Proc. Suppl.* **175** 155 (2008)
50. Atwood W B et al. *Astrophys. J.* **697** 1071 (2009); arXiv:0902.1089
51. Torii S, in *33rd Intern. Cosmic Ray Conf., 2–9 July 2013, Rio de Janeiro, Brazil* (Ed. A Saa) (2013) p. 631
52. Yoshitaka U et al., in *33rd Intern. Cosmic Ray Conf., 2–9 July 2013, Rio de Janeiro, Brazil* (Ed. A Saa) (2013) p. 2197
53. Totii S *PoS* **ICRC2015** 581 (2015)
54. Chang J et al. *Astropart. Phys.* **95** 6 (2017); arXiv:1706.08453
55. Yuhong Y et al. *Astropart. Phys.* **94** 1 (2017); arXiv:1703.00098
56. Qiao R et al. *Nucl. Instrum. Meth. Phys. Res. A* **886** 48 (2018)
57. Zhang Z et al. *Nucl. Instrum. Meth. Phys. Res. A* **836** 98 (2016); arXiv:1602.07015
58. Circella M (On behalf of the PAMELA Collab.) *Nucl. Instrum. Meth. Phys. Res. A* **518** 153 (2004)
59. Picozza P et al. *Astropart. Phys.* **27** 296 (2007)
60. Adriani O et al. *Nucl. Instrum. Meth. Phys. Res. A* **572** 471 (2007)
61. Orsi S (for the PAMELA Collab.) *Nucl. Instrum. Meth. Phys. Res. A* **580** 880 (2007)
62. Kounine A *Int. J. Mod. Phys. E* **21** 123005 (2012)
63. Aguilar M et al. (AMS Collab.) *Phys. Rev. Lett.* **110** 141102 (2013)
64. Binns W R et al., in *Origin Cosmic Rays. Proc. of the Symp., Bologna, Italy, June 11–14, 1980* (Dordrecht: D. Reidel Publ., 1981) p. 91
65. Binns W B et al. *Nucl. Instrum. Meth. Phys. Res.* **185** 415 (1981)
66. Müller D et al., in *Proc. of the 30th Intern. Cosmic Ray Conf. July 3–11, 2007, Merida, Yucatan, Mexico* Vol. 2 (Eds R Caballero et al.) (Mexico City, Mexico: Univ. Nacional Autonoma de Mexico, 2008) p. 83
67. Ave M et al. *Astrophys. J.* **678** 262 (2008)
68. Obermeier A et al. *Astrophys. J.* **742** 14 (2011); arXiv:1108.4838
69. Mitchell J W et al., in *32nd Intern. Cosmic Ray Conf., Beijing 2011, ICRC2011* (2011) ID 1234, https://doi.org/10.7529/ICRC2011/V06/1234; https://galprop.stanford.edu/elibrary/icrc/2011/papers.html
70. Binns W R et al. *Astrophys. J.* **788** 18 (2014)
71. Hams T et al. *PoS* **ICRC2015** 038 (2015)
72. Donnelly J et al. *Astrophys. J.* **747** 40 (2012)
73. Stone E C et al. *Space Sci. Rev.* **86** 285 (1998)

74. Wiedenbeck M E et al. *PoS* **ICRC2015** 340 (2015)
75. Binns W R et al., in *Proc. of the 30th Intern. Cosmic Ray Conf. July 3–11, 2007, Merida, Yucatan, Mexico* Vol. 6 (Eds R Caballero et al.) (Mexico City, Mexico: Univ. Nacional Autonoma de Mexico, 2008) p. 29
76. Smith L H et al. *Astrophys. J.* **180** 987 (1973)
77. Webber W R, Golden R L, Stephens S A, in *20th Intern. Cosmic Ray Conf.* Vol. 1 (1987) p. 325
78. Streitmatter E R et al., in *Proc. of the 21st Intern. Cosmic Ray Conf.* Vol. 3 (1990) p. 277
79. Bellotti R et al. *Phys. Rev. D* **60** 052002 (1999)
80. Menn W et al., in *Proc. of the 25th Intern. Cosmic Ray Conf., 30 July – 6 August, 1997, Durban, South Africa* Vol. 3 (Eds M S Potgieter, C Raubenheimer, D J van der Walt) (Transvaal, South Africa: Potchefstroom Univ., 1997) p. 409
81. Boezio M et al. *Astrophys. J.* **518** 457 (1999)
82. Sanuki T et al. *Astrophys. J.* **545** 1135 (2000)
83. Alcaraz J et al. (AMS Collab.) *Phys. Lett. B* **490** 27 (2000)
84. Boezio M et al. *Astropart. Phys.* **19** 583 (2003); astro-ph/0212253
85. Grigorov N L et al. *Sov. J. Nucl. Phys.* **11** 588 (1970); *Yad. Fiz.* **11** 1058 (1970)
86. Akimov V V "Izuchenie energeticheskogo spektra protonov pervichnykh kosmicheskikh luchei na ISZ 'PROTON-3'" ("Studies of the energy spectrum of protons in primary cosmic ways aboard PROTON-3 Earth satellite vehicle"), Candidate's Dissertation in Phys. and Math. Sci. (Moscow: Inst. of Nuclear Physics Lomonosov Moscow State Univ., 1973)
87. Ryan M J, Ormes J F, Balasubrahmanyan V K *Phys. Rev. Lett.* **28** 985 (1972)
88. Grigorov N L *Sov. J. Nucl. Phys.* **51** 99 (1990); *Yad. Fiz.* **51** 157 (1990)
89. Ivanenko I P et al. *Izv. Ross. Akad. Nauk Ser. Fiz.* **57** (7) 76 (1993)
90. Zatsepin V I et al. *Phys. Atom. Nucl.* **57** 645 (1994); *Yad. Fiz.* **57** 684 (1994)
91. Kawamura Y et al. *Phys. Rev. D* **40** 729 (1989)
92. Kawamura Y et al., in *Proc. of the 21st Intern. Cosmic Ray Conf.* Vol. 3 (1990) p. 89
93. Takahashi Y (for the JACEE Collab.) *Nucl. Phys. B Proc. Suppl.* **60** 83 (1998)
94. Asakimori K et al. *Astrophys. J.* **502** 278 (1998)
95. Derbina V A et al. *Astrophys. J.* **628** L41 (2005)
96. Zatsepin V I, Sokolskaya N V *Astron. Astrophys.* **458** 1 (2006); astro-ph/0601475
97. Panov A et al. *PoS* **ICRC2017** 1094 (2017)
98. Atkin E et al. *JETP Lett.* **108** 5 (2018); *Pis'ma Zh. Eksp. Teor. Fiz.* **108** 5 (2018) arXiv:1805.07119
99. Yue C et al. *PoS* **ICRC2017** 1076 (2017)
100. Gallo V et al. *PoS* **ICRC2017** 169 (2017)
101. An Q et al. (DAMPE Collab.) *Sci. Adv.* **5** eaax3793 (2019); arXiv:1909.12860
102. Alemanno F et al. (DAMPE Collab.) *Phys. Rev. Lett.* **126** 201102 (2021); arXiv:2105.09073
103. Kobayashi K, Marrocchesi P S et al. *PoS* **ICRC2021** 098 (2021)
104. Brogi P, Kobayashi K *PoS* **ICRC2021** 101 (2021)
105. Marrocchesi P S *PoS* **ICRC2021** 010 (2021)
106. Ahn H S et al. *Astrophys. J.* **707** 593 (2009); arXiv:0911.1889
107. Aguilar M et al. *Phys. Rep.* **894** 1 (2021)
108. Aguilar M et al. (AMS Collab.) *Phys. Rev. Lett.* **126** 041104 (2021)
109. Adriani O et al. (CALET Collab.) *Phys. Rev. Lett.* **125** 251102 (2020); arXiv:2012.10319
110. Adriani O et al. (CALET Collab.) *Phys. Rev. Lett.* **126** 241101 (2021); arXiv:2106.08036
111. Grebenyuk V et al. *Adv. Space Res.* **64** 2546 (2019)
112. Wu L et al. *PoS* **ICRC2021** 128 (2021)
113. Podorozhny D et al. *Adv. Space Res.* **70** 1529 (2022)
114. Turundaevskiy A N et al. *Adv. Space Res.* **70** 2696 (2022)
115. Alfaro R et al. (HAWC Collab.) *Phys. Rev. D* **96** 122001 (2017)
116. Vargas L H (for the HAWC Collab.) *EPJ Web Conf.* **208** 14001 (2019)
117. Varsi F et al. *PoS* **ICRC2019** 449 (2019)
118. Kudryashov I et al. *PoS* **ICRC2021** 166 (2021)
119. Kudryashov I et al. *Universe* **7** 460 (2021)
120. Fornieri O et al. *Phys. Rev. D* **104** 103013 (2021); arXiv:2007.15321
121. Yuan Q et al. *Front. Phys.* **16** 24501 (2021); arXiv:2007.01768
122. Fang K, Bi X-J, Yin P-F *Astrophys. J.* **903** 69 (2020); arXiv:2003.13635
123. Malkov M A, Moskalenko I V *Astrophys. J.* **911** 151 (2021); arXiv:2010.02826
124. Malkov M A, Moskalenko I V *Astrophys. J.* **933** 78 (2022); arXiv:2105.04630
125. Cowsik R et al. *Phys. Rev.* **158** 1238 (1967)
126. Ginzburg V L, Ptuskin V S *Sov. Phys. Usp.* **18** 931 (1975); *Usp. Fiz. Nauk* **117** 585 (1975)
127. Gaisser T K *Cosmic Rays and Particle Physics* (Cambridge: Cambridge Univ. Press, 1990)
128. Grebenyuk V et al., arXiv:1809.07285
129. Kudryashov I A et al. *Bull. Russ. Acad. Sci. Phys.* **87** 870 (2023); *Izv. Ross. Akad. Nauk Ser. Fiz.* **87** 927 (2023); arXiv:2303.16539
130. Strong A W, Moskalenko I V *Astrophys. J.* **509** 212 (1998)
131. Vladimirov A E et al. *Comput. Phys. Commun.* **182** 1156 (2011)
132. Bedugo J *PoS* **ICRC2021** 016 (2021)
133. Engelmann J J et al. *Astron. Astrophys.* **233** 96 (1990)
134. Adriani O et al. (CALET Collab.) *Phys. Rev. Lett.* **128** 131103 (2022); arXiv:2204.00845
135. Jones M D et al., in *Proc. of the 19th Intern. Cosmic Ray Conf.* Vol. 2 (1985) p. 28
136. Israel M H et al., in *Proc. of the 20th Intern. Cosmic Ray Conf., Moscow* Vol. 1 (1987) p. 330
137. Panov A D, Sokolskaya N V, Zatsepin V I *Nucl. Phys. B Proc. Suppl.* **256 – 257** 233 (2014)
138. Berezinskii V S et al. *Astrophysics of Cosmic Rays* (Amsterdam: North-Holland, 1990); Translated from Russian: *Astrofizika Kosmicheskikh Luchei* (Moscow: Nauka, 1984)
139. Castellina A, Donato F *Astropart. Phys.* **24** 146 (2005)
140. Strong A W, Moskalenko I V, Ptuskin V S *Annu. Rev. Nucl. Part. Sci.* **57** 285 (2007)
141. Blasi P *Astron. Astrophys. Rev.* **21** 70 (2013)
142. Grenier I A, Black J H, Strong A W *Annu. Rev. Astron. Astrophys.* **53** 199 (2015)
143. Berezhko E G et al. *Astron. Astrophys.* **410** 189 (2003); astro-ph/0308199
144. Aguilar M et al. (AMS Collab.) *Phys. Rev. Lett.* **117** 231102 (2016)
145. Panov A D et al. *Adv. Space Res.* **37** 1944 (2006)
146. Ahn H S et al. *Astropart. Phys.* **30** 133 (2008); arXiv:0808.1718
147. Adriani O et al. *Astrophys. J.* **791** 93 (2014); arXiv:1407.1657
148. Obermeier A et al. *Astrophys. J.* **752** 69 (2012); arXiv:1204.6188
149. Yue C et al. *PoS* **ICRC2021** 126 (2021)
150. Akaikea Y, Maestro P *PoS* **ICRC2021** 112 (2021)
151. Thoudam S, Hörandel J R *Mon. Not. R. Astron. Soc.* **435** 2532 (2013); arXiv:1304.1400
152. Binns W R et al. *Astrophys. J.* **324** 1106 (1988)
153. Vylet M et al., in *21st Intern. Cosmic Ray Conf.* Vol. 3 (1989) p. 19
154. Zatsepin V I et al. *Astron. Lett.* **35** 338 (2009); *Pis'ma Astron. Zh.* **35** 377 (2009)
155. Binns W R et al. *Astrophys. J.* **346** 997 (1989)
156. Israel M H et al., in *Intern. Cosmic Ray Conf., 18th, Bangalore, India, August 22 – September 3, 1983, Late Papers* Vol. 9 (Bombay: Tata Institute of Fundamental Research, 1983) p. 123
157. Lave K A et al. *Astrophys. J.* **770** 117 (2013)
158. Murphy R P et al. *Astrophys. J.* **831** 148 (2016); arXiv:1608.08183
159. Binns W R et al., in *Proc. of the 33rd Intern. Cosmic Ray Conf., Rio de Janeiro, 2013* (2013) ID 0646, URL: http://www.cbpf.br/~icrc2013/papers/icrc2013-0646.pdf
160. Lodders K *Astrophys. J.* **591** 1220 (2003)
161. Ellison D C, Drury L O'C, Meyer J-P *Astrophys. J.* **487** 197 (1997); astro-ph/9704293
162. Woosley S E, Heger A *Phys. Rep.* **442** 269 (2007); astro-ph/0702176
163. Israel M H et al. *Nucl. Phys. A* **758** 201 (2005)
164. Binns W R et al. *Astrophys. J.* **634** 351 (2005); astro-ph/0508398
165. de Nolfo G A et al. *Adv. Space Res.* **38** 1558 (2006); astro-ph/0611301
166. Israel M H et al. *PoS* **ICRC2015** 275 (2015)
167. Binns W R et al. *Science* **352** 677 (2016)
168. Kalyashova M E, Bykov A M, Osipov S M *Bull. Russ. Acad. Sci. Phys.* **85** 357 (2021); *Izv. Ross. Akad. Nauk Ser. Fiz.* **85** 482 (2021)

169. Vasil'ev O A et al. *Phys. Part. Nucl. Lett.* **18** 217 (2021); *Pis'ma Fiz. Elem. Chast. At. Yad.* **18** 233 (2021)
170. Adriani O et al. *Astrophys. J.* **770** 2 (2013); arXiv:1304.5420
171. Adriani O et al. *Astrophys. J.* **818** 68 (2016); arXiv:1512.06535
172. Bogomolov E A, Vasilyev G I *Bull. Russ. Acad. Sci. Phys.* **83** 967 (2019); *Izv. Ross. Akad. Nauk Ser. Fiz.* **83** 1066 (2019)
173. Bogomolov E A, Vasilyev G I, Menn W *Bull. Russ. Acad. Sci. Phys.* **85** 341 (2021); *Izv. Ross. Akad. Nauk Ser. Fiz.* **85** 466 (2021)
174. Aguilar M et al. (AMS Collab.) *Phys. Rev. Lett.* **123** 18102 (2019)
175. Ivanenko I P, in *23rd Intern. Cosmic Ray Conf., 19–30 July, 1993, Alberta, Canada, Invited, Rapporteur, and Highlight Papers* Vol. 2 (Eds D A Leahy, R B Hicks, D Venkatesan) (Singapore: World Scientific, 1993) p. 17
176. Podorozhnyi D, Turundaevskiy A *Adv. Space Res.* **59** 495 (2017)
177. Strong A W, Moskalenko I V *Astrophys. J.* **493** 694 (1998); astro-ph/9710124
178. Nishimura J et al., in *Proc. of the 25th Intern. Cosmic Ray Conf., 30 July–6 August, 1997, Durban, South Africa* Vol. 4 (Eds M S Potgieter, C Raubenheimer, D J van der Walt) (Transvaal, South Africa: Potchefstroom Univ., 1997) p. 233
179. Abdollahi S et al. (The Fermi-LAT Collab.) *Phys. Rev. D* **95** 082007 (2017); arXiv:1704.07195
180. Ambrosi G et al. (DAMPE Collab.) *Nature* **552** 63 (2017); arXiv:1711.10981
181. Adriani O et al. (CALET Collab.) *Phys. Rev. Lett.* **120** 261102 (2018); arXiv:1806.09728
182. Aguilar M et al. (AMS Collab.) *Phys. Rev. Lett.* **122** 101101 (2019)
183. Chang J et al. *Nature* **456** 362 (2008)
184. Panov A D et al. *Astrophys. Space Sci. Trans.* **7** 119 (2011) https://doi.org/10.5194/astra-7-119-2011
185. Borisov S V et al. *Bull. Lebedev Phys. Inst.* **37** 184 (2010); *Kratk. Soobshch. Fiz. FIAN* **37** (6) 35 (2010)
186. Aharonian F et al. *Astron. Astrophys.* **508** 561 (2009); arXiv:0905.0105
187. Borla Tridon D et al., in *Proc. of the 32nd Intern. Cosmic Ray Conf., ICRC2011, 11–18 August, 2011, Beijing, China* Vol. 6 (2011) p. 47, https://doi.org/10.7529/ICRC2011/V06/0680; arXiv:1110.4008
188. Archer A et al. (The VERITAS Collab.) *Phys. Rev. D* **98** 062004 (2018); arXiv:1808.10028
189. Ding Y-C *Phys. Rev. D* **103** 115010 (2021); arXiv:2007.00703
190. Panov A D et al. *Bull. Russ. Acad. Sci. Phys.* **75** 319 (2011); *Izv. Ross. Akad. Nauk Ser. Fiz.* **75** 348 (2011)
191. Adriani O et al. *Nature* **458** 607 (2009); arXiv:0810.4995
192. Ackermann M et al. (Fermi LAT Collab.) *Phys. Rev. Lett.* **108** 011103 (2012); arXiv.1109.0521
193. Aguilar M et al. (AMS Collab.) *Phys. Rev. Lett.* **110** 141102 (2013)
194. Accardo L et al. (AMS Collab.) *Phys. Rev. Lett.* **113** 121101 (2014)
195. Adriani O et al. *Phys. Rev. Lett.* **111** 081102 (2013); arXiv:1308.0133
196. Haino S et al., in *Proc. of the 29th Intern. Cosmic Ray Conf., August 3–10, 2005, Pune, India* Vol. 3 (Eds B Sripathi Achary et al.) (Mumbai: Tata Institute of Fundamental Research, 2005) p. 13
197. Abe K et al. (BESS Collab.) *Phys. Lett. B* **670** 103 (2008); arXiv:0805.1754
198. Adriani O et al. *JETP Lett.* **96** 621 (2013); *Pis'ma Zh. Eksp. Teor. Fiz.* **96** 693 (2012)
199. Aguilar M et al. (AMS Collab.) *Phys. Rev. Lett.* **117** 091103 (2016)
200. Mayorov A G et al. *JETP Lett.* **93** 628 (2011); *Pis'ma Zh. Eksp. Teor. Fiz.* **93** 704 (2011)
201. Ding Y-C, Li N, Zhou Y-F *JCAP* **2023** (03) 051 (2023); arXiv:2212.02539
202. Poulin V et al. *Phys. Rev. D* **99** 023016 (2019); arXiv:1808.08961
203. Walsh N, Rauch B, Zober W, in *43rd COSPAR Scientific Assembly. Held 28 January–4 February, 2021* (2021) p. 1357
204. Rauch B, Walsh N, Zober W *PoS* **ICRC2021** 087 (2021)
205. Perrina C (on behalf of the HERD Collab.) *EPJ Web Conf.* **280** 01008 (2023)
206. Karmanov D et al. *Adv. Space Res.* **64** 2619 (2019)
207. Kurganov A et al., arXiv:2306.13406
208. Wefel J P et al., in *Proc. of the 29th Intern. Cosmic Ray Conf. August 3–10, 2005, Pune, India* Vol. 3 (Eds B Sripathi Acharya et al.) (Mumbai: Tata Institute of Fundamental Research, 2005) p. 105
209. Sanuki T et al., astro-ph/0002481
210. Adams G et al. *Bull. Russ. Acad. Sci. Phys.* **61** 922 (1997); *Izv. Ross. Akad. Nauk Ser. Fiz.* **61** 1181 (1997)
211. Arqueros F et al. (HEGRA Collab.) *Astron. Astrophys.* **359** 682 (2000); astro-ph/9908202
212. Roth M et al., in *Proc. of the 28th Intern. Cosmic Ray Conf. July 31–August 7, 2003, Tsukuba, Japan* Vol. 1 (Eds T Kajita et al.) (2003) p. 139
213. Kieda D et al., in *Proc. of the 26th Intern. Cosmic Ray Conf., August 17–25, 1999, Salt Lake City, Utah, USA* Vol. 3 (Eds D Kieda, M Salamon, B Dingus) (1999) p. 191
214. Fowler J W et al. *Astropart. Phys.* **15** 49 (2001); astro-ph/0003190
215. Binns W R et al. *Astrophys. J.* **936** 13 (2022)